

Supplementary Materials for

Social network plasticity decreases disease transmission in a eusocial insect

Nathalie Stroeymeyt*, Anna V. Grasse, Alessandro Crespi, Danielle P. Mersch,
Sylvia Cremer*, Laurent Keller*

*Corresponding author. Email: laurent.keller@unil.ch (L.K.); nathalie.stroeymeyt@normalesup.org (N.S.);
sylvia.cremer@ist.ac.at (S.C.)

Published 23 November 2018, *Science* **362**, 941 (2018)
DOI: 10.1126/science.aat4793

This PDF file includes:

Materials and Methods
Figs. S1 to S15
Tables S1 to S5
References

Materials and Methods

Ant host

All experiments were performed using the common garden ant *Lasius niger*. Colonies were initiated from newly mated queens collected on the University of Lausanne campus, Switzerland (46.521016, 6.575189) in July 2013 and June 2014. Colonies were reared at constant temperature (25°C) with 55% humidity and a 12h/12h light/dark cycle. They were given water *ad libitum* and fed weekly with diluted honey, mealworms and artificial ant diet (29). Colonies were between 4.5 and 16 months old at the time of the experiments, and each colony contained a single queen, between 32 and 193 workers, between 10 and 152 larvae, between 0 and 33 pupae, and a small egg pile (1st quartile/median/3rd quartile: 85/107/128 workers; 39/57/80 larvae; 0/1/9 pupae; n=44). In a subset of 11 colonies founded in 2013, all newly-emerged workers were paint-marked every fortnight from the emergence of the first workers following a well-established protocol for paint-marking small ants (30), so that each age cohort was identified by a unique color combination ('age-marked colonies'). All experiments complied with Swiss law and the institutional guidelines of the University of Lausanne.

Fungal pathogen

We used the generalist entomopathogenic fungus *Metarhizium brunneum* (strain MA275, KVL 03-143). *M. brunneum* is a natural pathogen of *Lasius* ants (12, 17) and is frequently found in the soil of these ants' habitat (18, 31, 32). The ants can contract the disease by physical contact with sporulating insect bodies, which produce large amounts of infectious conidiospores (hereafter referred to as spores; c. 12 million per cadaver in ants (25)). Aliquots of the fungal spores were kept in long-term storage at -80°C. Prior to the experiment the spores were grown on Sabouraud Dextrose Agar culture medium at 23°C and harvested by suspending them in 0.05% sterile Triton

X-100 solution (Sigma). The germination rates of the spore suspensions were determined directly before the start of each experiment and were above 90%. Fungal exposure was performed by applying a 0.5 μ L droplet of spore suspension (10^9 spores/ml) onto the ants' gaster (abdomen), whereas sham exposure was performed by applying a 0.5 μ L droplet of 0.05% sterile Triton-X100 only. Approximately 500,000 spores were thus applied on each ant in the fungal exposure treatment. As only 10-15% of spores typically adhere to the ant's cuticle with this exposure method (12), this should correspond to an effective exposure dose of c. 50,000-75,000 spores. This is much lower than the amount of spores encountered in the wild on sporulating insect bodies (c. 12×10^6 per cadaver (25)). In our survival experiment (see below), this exposure load was associated with a mortality of 89% among treated foragers over the 9 days following treatment (Fig. S11).

Quantification of pathogen load

Individual pathogen load was determined by quantitative real-time PCR (qPCR), as described in Giehr et al (2017) (33). At the end of the experiment, each colony was immediately frozen on dry ice to prevent additional ant-to-ant fungal transfers. Each ant was identified by manually scanning its tag, then placed in an individual extraction tube, and stored at -80°C until DNA extraction. Prior to DNA extraction, the samples were homogenized using a TissueLyser II (Qiagen) with a mixture of 2.8 mm ceramic (VWR), 1 mm zirconia (BioSpec Products) and 425-600 μ m glass beads (Sigma-Aldrich). Homogenization was carried out in two steps (2 x 2 min at 30 Hz). DNA extraction was performed using Qiagen DNeasy 96 Blood & Tissue Kit (Qiagen, Hilden, Germany) and following the manufacturer's instructions, with a final elution volume of 50 μ l. qPCR was performed using primers designed to bind to the *Metarhizium brunneum* ITS2 rRNA gene region (Met-ITS2-F: 5'- CCCTGTGGACTTGGTGTG-3', Met-ITS2-R: 5'- GCTCCTGTTGCGAGTGTGTTT-3') (33). Reactions were performed in 20 μ l volumes using 1x

KAPA SYBR® FAST qPCR Master Mix (Kapa Biosystems), with 3 pmol of each primer (Sigma-Aldrich), and 2 μ l of extracted DNA. The amplification program was initiated with a first step at 95°C for 5 min, followed by 40 cycles of 10 s at 95°C and 30 s at 64°C. Quantification was done based on the standard curve method, using standards covering a range from 10^{-1} to 10^{-5} ng/ μ l fungal DNA (measured using a NanoDrop spectrophotometer). The standard with the lowest concentration was determined to be the detection threshold. Samples as well as standards were run in triplicates and each run included a negative control. Specificity was confirmed by performing a melting curve analysis after each run. Fungal load determination was performed on all individuals in pathogen-exposed colonies, and on 10 randomly chosen individuals in sham-exposed colonies. The latter confirmed the absence of *M. brunneum* in sham-exposed colonies, also indicating that there was no natural, baseline infection with *M. brunneum* within colonies prior to the experiment.

To establish a quantitative relationship between the fungal DNA concentrations produced by the qPCR analysis and the corresponding number of spores on the body of each ant, we used calibration data in which the DNA concentration of four replicate suspensions (50 μ L 0.05% Triton-X 100 containing 1.49×10^8 *M. brunneum* conidiospores) was determined using the NanoDrop spectrophotometer. The measured concentrations ranged from 154.8 to 220.3 ng/ μ l fungal DNA (mean \pm standard deviation: 185.2 ± 26.9 ng/ μ L; coefficient of variation: 14.5%), providing a mean to convert our qPCR results from fungal DNA concentration to number of spores:

$$N_{ant} = (C_{ant} \times V_{ant}) \cdot \frac{N_{suspension}}{C_{suspension}^* \times V_{suspension}},$$

where N_{ant} is the number of spores on the body of the sampled ant, C_{ant} is the fungal DNA concentration of the sampled ant directly measured by qPCR, V_{ant} is the elution volume used for the qPCR analysis, $N_{suspension}$ is the number of spores in the calibrating suspensions (1.49×10^8),

C^* _{suspension} the mean fungal DNA concentration determined by NanoDrop (185.2 ng/ μ L), and $V_{suspension}$ the volume of the calibrating suspensions. As the qPCR elution volume and the volume of the calibrating suspensions were the same in our experiments (50 μ L), this formula can be simplified as follows: $N_{ant} = C_{ant} \times 8.04 \times 10^5$ spores. μ L.ng⁻¹. This conversion suggests that the simulation-derived threshold value (Fig. 3A) used to distinguish high from low loads, which was estimated to be equivalent to a real load of 4.32×10^{-5} ng/ μ L fungal DNA (Fig. 2A), would correspond to c. 35 spores on an ant's body. Interestingly, this dose corresponds to a LD2 ('lethal dose 2%', i.e., exposure dose that leads to 2% excess mortality in isolated workers) in the *Lasius neglectus* – *Metarhizium brunneum* host-pathogen system (Table S4). However, we would like to stress that this estimation is likely to be very imprecise because of a significant degree of uncertainty in each step of the conversion, and should therefore be considered as indicative of an order of magnitude for the biological equivalent of our simulation-derived threshold, rather than as an exact value.

Automated behavioral tracking

The behavior of each ant was recorded using the automated ant tracking system developed by Mersch et al (2013) (5), which was adapted to record ants under a glass cover while avoiding light reflection effects. This was achieved by modifying the orientation of the infra-red light emitting diodes (LED), which were positioned to the side of the system and emitted light diagonally rather than vertically. The tracking system is based on the automatic detection of small paper tags bearing unique two-dimensional matrix barcodes from the ARTag library (34), which are glued to the thorax of each ant. Ants easily carry loads weighing several times their own body weight (35, 36). Each tag weighed each approximately 0.12mg, which corresponds to about 10% of a worker's body weight. Visual observations in preliminary tagging trials showed that tagged ants exhibited

normal behavior, participating in all tasks and interacting with each other and untagged workers without apparent bias. Their activity levels and resting behavior also appeared similar to that of untagged ants.

The tags were detected and identified in real time by the tracking system, which records the location and orientation of each ant twice per second (Fig. S1). The rate of tag loss in our experiments was lower than 0.075% per ant and per day, and the detection rate was $92.7 \pm 0.2\%$ per ant and per second, which allowed us to obtain exhaustive behavioral records for each individual.

Experimental arenas

Experiments were carried out in rectangular arenas (103×70mm) with Fluon-coated walls to prevent the ants from escaping. Each arena was divided into a nesting area (70×40 mm) and a foraging area (70×54 mm) separated by a 9mm-thick wall with a rectangular entrance hole (4×3mm) to allow the ants to pass. The foraging area was not covered with a top lid. By contrast, the nesting area (6mm height) was covered with an infrared (IR) transmitting glass filter (Hoya Sharp-Cut Color Glass Filter R-64), which blocked all wavelengths shorter than 620nm. The filter ensured that the nest interior appeared dark to the ants while allowing automated behavioral tracking inside the nest. Water and 10% sugar water were provided *ad libitum* via two cotton-stoppered plastic tubes connected to underneath containers, and whose opening was level with the foraging area's floor (Fig. S1).

Main experiment

The main experiment aimed at uncovering the social organization and network structure of healthy colonies ($n=22$), and the changes induced by exposure to an infectious pathogen. At the beginning of each experimental trial, all workers and the queen from a colony were individually marked under light CO₂ anesthesia by affixing a unique tag (workers: 0.7mm tags; queens: 1.6mm tags)

onto their thorax using a droplet of solvent-free instantaneous superglue (Pattex Power Easy Gel). After tagging, each ant was isolated in an individual Eppendorf tube for 10 min before being released. Twenty-four hours after tagging, the entire colony was transferred into an experimental arena, which was placed into a tracking chamber (5) with artificially controlled conditions (60% humidity, day-night cycle of 12h light at 26°C from 6am to 6pm UTC, and 12h darkness at 22°C from 6pm to 6am). Automated tracking was started after one night of acclimatization to the system, and lasted until the end of the experiment (five days in total). Colonies were left undisturbed for four days ('*pre-treatment period*'), then subjected either to a control treatment (exposure of to a sham solution; n=11 colonies) or to a pathogen exposure treatment (exposure to a fungal spore suspension; n=11 colonies). Colonies were matched for size and age between treatments (mean± standard error: fungal treatment, 1 queen, 122±10 workers, 52.0±8.2 larvae and 8.2±1.8 pupae, 8.7±1.4 months old; sham control: 1 queen, 108±8.2 workers 47.4±10.0 larvae and 14.3±3.5 pupae, 6.8±1 months old; Welch Two Sample t-tests, No. workers: $t=1.086$, $df=19.28$, $p=0.29$; No. larvae: $t=-0.36$, $df=19.25$, $p=0.72$; No. pupae: $t=1.55$, $df=14.98$, $p=0.14$; colony age: $t=1.1093$, $df=17.38$, $p=0.28$), and treatments were alternated across successive trials to avoid temporal biases. Treatment was performed individually on 10% of the colony's workers, which were gently collected from the foraging arena using a clean, fine paintbrush. Because the foraging arena did not have a roof cover, this collection procedure caused minimal disturbance to the rest of the colony. Collected ants were exposed to either the fungal spore suspension or the sham solution, as described above, and then gently returned to the center of the foraging arena. All treatments were performed at the same time of day (between 9 and 10 am UTC). As the exposure procedure may disrupt the behavior of treated foragers and their nestmates, we allowed all colonies a recovery phase of two hours after treatment. After that, behavioral tracking was continued for twenty-four

additional hours ('*post-treatment period*'), at which time all ants were individually frozen at -80°C for fungal load determination, as described above. During this early period following fungal contamination, spores are known to be transferred upon physical contacts between nestmates (19, 24). Spores later penetrate into the host's body and start replicating with a time delay of 1 to 2 days after first contact with the host's cuticle (22, 37, 38). Because individual fungal loads were measured at 26h, that is, *before* the fungus has had time to cause an internal infection, they should closely reflect the level of cross-contamination among colony members arising from social contacts between contaminated ants and their nestmates (19).

Age experiment

This experiment aimed at testing the hypothesis that younger workers are less likely to be contaminated with pathogens brought back to the nest by foragers than older workers (14). To do so, we used the 11 age-marked colonies mentioned above and applied the same experimental protocol as in the main experiment. However, as we were interested in determining inter-individual variation in contamination risk within pathogen-exposed colonies, we did not use a sham control, but instead exposed all colonies to the pathogen suspension. We then used qPCR to determine individual fungal load one day after treatment as a function of age.

Survival experiment

This experiment aimed at investigating the longer-term biological consequences of early contamination with *M. brunneum*. To do so, we exposed 11 colonies to the pathogen suspension using the same experimental protocol as in the main experiment. However, instead of interrupting the experiment one day after the recovery period, we allowed the disease to develop and monitored individual survival for nine days (i.e., long enough for *M. brunneum* to spread in the colony and kill primary and secondarily infected individuals, but before sporulation occurs (22)).

General analysis procedure

Colonies showed consistent, steady changes in behavior during the four pre-treatment days, which presumably reflect their progressive habituation to the experimental arena (39). The last day before treatment was thus more relevant for comparisons with the post-treatment period than the whole pre-treatment period. We therefore only considered the final day before treatment in analyses involving the pre-treatment period.

Behavioral data were aggregated over successive periods of 3 hours, which constituted the basic unit of the analysis. This allowed us to account for the strong circadian rhythms displayed by the ant colonies by including time of day as a random factor in our statistical analyses (see below).

Because network properties scale with network size (40), and because individual behavior is strongly affected by imminent death (41), we excluded all individuals that died before the end of the experiment from the analysis. As *M. brunneum* does not cause death within the time span covered by our experiment, we expect these ants to have died from a disease-independent cause. In agreement with this prediction, the proportion of ants that died (and were thus excluded from the analysis) was similar in sham-treated and pathogen-exposed colonies (Treated foragers, sham-treated colonies: $18.2 \pm 7.2\%$, pathogen-exposed colonies: $13.9 \pm 4.6\%$, Welch Two Sample t-test: $t=0.51$, $df= 16.9$, $p=0.62$; Untreated nestmates, sham-treated colonies: $9.7 \pm 1.9\%$, pathogen-exposed colonies: $11.5 \pm 1.7\%$, Welch Two Sample t-test: $t=-0.73$, $df=19.6$, $p=0.47$). This led to the following final sample sizes in analyses; sham-treated colonies: 11 queens, 685 nurses, 284 untreated foragers and 94 treated foragers; pathogen-exposed colonies: 11 queens, 862 nurses, 214 untreated foragers and 105 treated foragers.

Note that all data collection and analyses were performed using automated methods (automated tracking, qPCR and unique pipeline of C++ and R programs), and were thus not subject to potential observer bias.

Spatial analysis

The individual trajectories produced by the automated tracking system were first used to determine each worker's task group: workers that remained inside the nest throughout the pre-treatment period were classified as 'nurses' whereas workers that left the nest at least once during the pre-treatment period were classified as 'foragers'. For each ant, we extracted the proportion of time spent inside the nest by calculating the proportion of coordinates falling within the nest among all detected locations. In each colony, frequent foragers were defined as the 50% of foragers spending the highest proportion of their time outside the nest, and occasional foragers as the 50% of foragers spending the lowest proportion of their time outside the nest. To quantify individual activity, we used change-point detection to identify the times when the mean and variance of each ant's speed exhibited a regime shift (42), thus delimiting successive homogeneous trajectory segments or 'bouts'. We then used cluster analysis to classify bouts. These fell into two broad categories: high speed and low turn angles ('active' bouts), and low speed and high turn angles ('inactive' bouts). This allowed us to measure the proportion of time an ant spent in an active state. In addition, we extracted the total distance moved from each ant's total trajectory. To evaluate the area over which each ant moved when within the nest, we used the R package *adehabitatHR* to calculate its home range, that is, the smallest area in which the ant spends 95% of its time (43). This calculation was done over the ant's within-nest portion of the trajectory ('nest area visited', Fig. S14). Finally, to quantify the degree of spatial overlap between ants and/or groups of ants, we calculated their Bhattacharyya's affinity index as described by Fieberg and Kochanny (2005) (43), which ranges

from 0 (no overlap between the two ants/groups' spatial distribution) to 1 (identical spatial distributions).

Social network analysis

To build each colony's social contact networks, we inferred physical contacts between ants using a geometrical approach adapted from Mersch et al (2013) (5), in which each ant was represented by a trapezoid extending from the ant's mouthparts to the end of its gaster. We considered three alternative methods for contact inference, whereby a contact was recorded if the front end of one ant's trapezoid was located within another ant's trapezoid ('*front contacts*', Fig. 1), if the front end or the back end of one ant's trapezoid was located within another ant's trapezoid ('*front and back contacts*'), or if the trapezoids representing two ants overlapped in any way ('*any overlap*'). Uninterrupted contacts in which both ants remained stationary (i.e., moved by less than a third of the ant's body length, i.e., by less than 0.6mm between successive records) were considered as a single contact and their duration was recorded. To avoid giving disproportionate weight to overlong contacts in which both ants are resting, long-lasting contacts involving immobile ants (c. 2% of all contacts) were truncated after 2 minutes. In order to evaluate the effect of this truncation and to determine which of the three contact inference methods was most appropriate to study the transmission of *M. brunneum* spores in *L. niger* colonies, we parameterized our simulation model for each inference method with and without contact truncation, and quantified the fit between the simulation outcome and the experimental pathogen load data (qPCR). The '*front contacts*' method with truncation provided the best fit and was thus retained for all other analyses (see section 'Simulations' below for detail).

Untreated workers were divided into three equal groups based on their total duration of contact with treated workers during the first day after treatment (low, medium and high contact

with treated workers). Some analyses were performed separately for nurses and for workers that had low direct contact with treated workers to underscore the value of using a whole network approach to predict individual contamination and mortality risks in the non-trivial case of minimal direct contact with pathogen-exposed ants (Figs. S10-S11).

Contact records were used to build time-aggregated weighted contact networks in which each node represents an ant and each weighted edge represents the cumulated duration of contact between a pair of ants over each three-hour window. Throughout the paper, these contact networks are represented using layouts produced by the Fruchterman-Reingold Algorithm. Networks were analyzed in R using the dedicated package *igraph*. This allowed us to determine the following properties for each weighted network (or for each node within the weighted network):

- **Modularity:** degree of compartmentation of the network into communities, that is, well-separated groups of tightly connected nodes (8). We used the Louvain method for modularity optimization of weighted networks (44), in which modularity is defined as:

$$Q = \frac{1}{2m} \sum_{ij} \left[A_{ij} - \frac{k_i k_j}{2m} \right] \cdot \delta(c_i, c_j),$$

where Q is the modularity; A_{ij} the edge weight between nodes i and j ; k_i and k_j the sum of the weights of the edges attached to nodes i and j , respectively; $2m$ the sum of all of the edge weights in the network; c_i and c_j the communities of nodes i and j , and δ a simple delta function, defined as:

$$\delta(x, y) = \begin{cases} 0 & \text{if } x \neq y \\ 1 & \text{if } x = y \end{cases}.$$

- **Clustering coefficient:** tendency of the neighboring nodes of any given node to also be connected to one another, i.e., to form a clique (fully connected set of nodes). This was measured as the average of the local weighted clustering of each node, as defined by A. Barrat (45):

$$C_i = \frac{1}{s_i(k_i - 1)} \sum_{j,h \neq i} \left[\frac{(w_{ij} + w_{ih})}{2} a_{ij} a_{ih} a_{jh} \right],$$

where C_i is the weighted clustering coefficient of node i , s_i the strength of node i (i.e., the sum of the weights of all edges connected to i), k_i the degree of node i (i.e., the number of edges connected to i), w_{ij} and w_{ih} the weights of the edges connecting i to j and h , respectively, and a_{ij} , a_{ih} and a_{jh} are elements of the adjacency matrix, defined as:

$$a_{xy} = \begin{cases} 1 & \text{if there is an edge between } x \text{ and } y \\ 0 & \text{if there is no edge between } x \text{ and } y \end{cases}.$$

- **Density:** proportion of realized connections among all possible connections
- **Diameter:** maximum path length within the network. For each pair of nodes, path length is defined as the weighted length of the shortest path linking those nodes. All shortest paths between all pairs of nodes were determined using Dijkstra's algorithm for weighted networks. Because Dijkstra's algorithm considers edge weights as geodesic distances rather than as connection strengths, in this instance edge weights were defined as the reciprocal of the cumulated duration of contact between each pair of ants (i.e., $\frac{1}{\text{contact duration}}$). Once the shortest path between two nodes was determined, the corresponding path length was calculated as the sum of the edge weights along that path.
- **Network efficiency:** average connection efficiency of all pairs of nodes, where connection efficiency is the reciprocal of the shortest path length between the two nodes
- **Degree:** number of edges connected to a node
- **Task assortativity:** degree of preferential association between workers of the same task group (either nurses or foragers, defined as explained above). Task assortativity was calculated using Newman's method (46, 47):

$$r = \frac{\sum_t e_{tu} - \sum_t a_t b_t}{1 - \sum_t a_t b_t},$$

where e_{tu} is the fraction of edges connecting ants of task group t to ants of task group u ,

$$a_t = \sum_u e_{tu} \text{ and } b_u = \sum_t e_{tu}.$$

Contact randomization

Randomizations were performed directly on the time-ordered sequence of contacts; null-model random networks were then obtained by building the time-aggregated network corresponding to each randomized sequence. Randomizations were performed following the ‘Randomized Edges’ method described by Holme & Saramäki (2012) (48). All observed time-ordered contacts were considered sequentially. For each focal contact, another ‘alternative’ contact was picked at random within the contact sequence, and one ant from the focal contact was randomly swapped with one ant from the alternative contact. If the swap resulted in a self-contact (i.e., an ant interacting with itself) or a multiple contact (i.e., two temporally overlapping contacts between the same two ants), then it was undone and another ‘alternative’ contact was picked, until the swap fulfilled both conditions. This randomization procedure conserves the temporal properties of the contact sequence (time stamp and duration of each contact) and the total number of contacts for each individual, while randomizing contact partners, which allows the effect of network topology (i.e. distribution of contacts) to be tested independently of any temporal effects. We wrote a custom C++ program implementing this algorithm, and produced 100 randomized sequences for each observed contact sequence.

Simulations

We used a temporally-explicit stochastic model to simulate the transmission of fungal spores over the time-ordered contact sequences, which is appropriate as their transmission can occur over single contact events (49). Simulations were performed on observed and randomized contact sequences collected either on the last day before treatment (*'pre-treatment'* simulations), or on the first day after treatment, after the two-hour recovery period (*'post-treatment'* simulations). Our simulation model was based on standard temporal Susceptible-Infectious epidemiological models (50, 51). However, because the time span of our simulations was shorter than the time necessary for the pathogen to start replicating, we modified the standard Susceptible-Infectious model in two major ways: first, the total quantity of spores in the system remained constant throughout the simulation (no replication); second, infectiousness depended on the amount of spores carried by each ant at the time of contact. For simplicity we refer to spore-carriers as ‘infectious’ ants and non-carriers as ‘susceptible’ ants. Simulations started with a set of initially infectious ants, which corresponded either to the experimentally-treated ants, or to the same number of ants selected randomly from a subset of individuals with specific properties (e.g., high degree ants or frequent foragers). At the onset of simulations, infectious individuals were given an arbitrary load of 1, whereas susceptible individuals were given a load of 0. All time-order contacts were then considered sequentially. Any contact involving at least one infectious individual with a load above the infectiousness threshold θ could result in directional spore transmission from the ant with the higher load (‘source’) to the ant with the lower load (‘target’). Transmission was a stochastic event occurring at a probability $\beta \cdot \lambda_s$, where β is the probability of transfer and λ_s the load of the source individual, reflecting the fact that ants carrying larger amounts of spores are more likely to transfer

them to nestmates. If transmission occurred, the amount of spores transferred T was calculated according to the following formula:

$$T = \frac{\Delta\lambda_{ini}}{2} - (1 - 2\gamma)^d \cdot \frac{\Delta\lambda_{ini}}{2} \quad (1),$$

where T is the total amount transferred, $\Delta\lambda_{ini}$ is the difference in load between the two ants (load of the source minus the load of the target) at the beginning of the contact, γ the transmission rate, and d the duration of the contact. This equation calculates the total amount of spores transferred under the assumption that at each unit time step i , the ants exchange a load of $\gamma \cdot \Delta\lambda_i$, where $\Delta\lambda_i$ is the difference in load between the two ants at time step i . According to this model, the rate of spore transfer progressively decreases during a single contact. In addition, an infinitely long contact should theoretically result in the homogenization of the load of both ants. Once the amount of spores transferred was determined, the load of both source and target ants was updated accordingly (i.e., T was added to the target ant's load and subtracted from the source ant's load) and the next contact in the sequence was considered. This stochastic process was repeated until the end of the contact sequence. For each simulation, we recorded the time at which each susceptible individual first received spores (first transfer time), the final load of each individual, and the mean, variance and skewness of the final distribution of loads among originally susceptible individuals. To obtain an objective measure of spore transmission rate, we further fit a r-K logistic equation (52) over first transfer times and determined the growth rate r . These values were averaged over 500 simulations for each contact sequence.

The infectiousness threshold θ was determined based on preliminary trials which showed that ants exposed to as few as 120 spores could lead to detectable transmission using the qPCR method. Our experimentally-exposed individuals received on average 5×10^5 spores ($0.5 \mu\text{L}$ at a concentration of $10^9 \text{ spores.mL}^{-1}$), which corresponded to a load of 1 in our simulation model. We

therefore used an infectiousness threshold $\theta = \frac{120}{5 \cdot 10^5} = 0.00024$. To parameterize the probability

of transfer β and the transmission rate γ , we used the automated tracking system to monitor 50 short encounters between one freshly fungal-treated ant and one susceptible nestmate ($n=5$ colonies; 10 encounters per colony). In each encounter, the two ants were placed in a small Fluonized Petri dish (5 cm in diameter) and allowed to explore and interact freely for a total duration of five minutes, then they were immediately frozen at -80°C for fungal load determination, as described above. In 38 out of 50 encounters, contact between the two ants led to the transfer of a detectable amount of spores from the fungal-exposed to the susceptible ant, while in the other 12 encounters, no spores could be detected on the susceptible ant. We then used the tracking data to determine the total number of contacts that took place during each five-minute encounter ('*front contacts*': range 0-10, median 3 contacts; '*front and back contacts*': range 0-14, median 3; '*any overlap*': range 1-21, median 6), and their cumulated duration ('*front contacts*': range 0-65, median 9 seconds spent in contact; '*front and back contacts*': range 0-99, median 9; '*any overlap*': range 0.5-162.5, median 20). We first parameterized the probability of transfer β by considering whether spore transfer had taken place or not depending on the number of contacts between the two ants.

Assuming each contact is associated with a probability β of transmission, then the probability that no spores are transferred during an encounter e involving N_e contacts is $p_{no_transfer} = (1-\beta)^{N_e}$.

Conversely, the probability that spores are transferred during such an encounter is $p_{transfer} = 1 - (1-\beta)^{N_e}$. For each encounter, it is therefore possible to determine the probability of obtaining the observed outcome as a function of β . We then calculated the overall likelihood of our results for each possible value of β ranging between 0 and 1 with an incremental step of 0.01 by multiplying the probability of obtaining the observed outcome across all encounters. We

selected the parameter value of β that maximized the likelihood of our results ('*front contacts*': $\beta=0.39$; '*front and back contacts*': $\beta=0.36$; '*any overlap*': $\beta=0.23$). For each encounter e , we then used formula (1) to calculate the predicted amount of transferred spores for each possible value of $\gamma=10^\gamma$, where γ ranged from -5 to -1/3 with an incremental step of 0.0001. For this, we used the following input values: $d_e = \beta \cdot D_e$, where D_e is the cumulated duration of contact between the two ants in encounter e ; $\lambda_t = 0$ (target ant initially susceptible); and $\lambda_s = L_s + L_t$, where L_s and L_t are the respective loads of the source and target ants at the end of the encountered, as determined by qPCR. We selected the value of γ that minimized the sum of squared residuals between predicted (i.e., calculated) and observed (i.e., measured by qPCR) values across all encounters ('*front contacts*': $\gamma=0.00066$; '*front and back contacts*': $\gamma=0.00072$; '*any overlap*': $\gamma=0.00069$).

In the time window covered by our simulations, which is too short for pathogen replication to start, a significant amount of spores are actively removed by workers through self-grooming and allo-grooming. These processes could not be quantified by automated tracking, and were therefore not included in the simulation model, so the simulation results likely over-estimate the pathogen load on each individual.

To evaluate the predictive value of our simulation model, we fitted a general linear model between simulated pathogen loads (outcome of simulations run over the full 2-hour recovery period + 24 hours until freezing) and observed pathogen loads (measured by qPCR) for each of the 22 colonies exposed to fungal spores that were frozen one day after treatment (fungal spore treatment in main experiment, $n=11$, and age experiment, $n=11$), as well as one general linear mixed model with colony identity as a random factor for the 22 colonies pooled. Both simulated load and observed load were log-transformed to ensure normality of the model residuals. We then compared the AIC and R^2 of each model depending on the type of contact inference method used

(‘*front contacts*’ vs. ‘*front and back contacts*’ vs. ‘*any overlap*’) and on whether the contacts had been truncated or not (see Table S5 for detail; lower AIC values indicate a better fit). Contact truncation improved the fit between simulated and experimental data in a majority of colonies (‘*front contacts*’: 14 out of 22; ‘*front and back contacts*’: 16 out of 22; ‘*any overlap*’: 20 out of 22) and in the pooled fits. In addition, the ‘*front contacts*’ method led to a better fit between simulated and experimental data than either the ‘*front and back contacts*’ method or the ‘*any overlap*’ method in the majority of colonies (13 out of 22), and in the pooled fits. We thus retained the truncated, ‘*front contacts*’ method for all simulations and analyses. Our simulation model was highly predictive the experimental data (Fig. 2, Table S5), and outperformed three simpler models in which individual pathogen load or worker survival was predicted by whether or not an ant had been in contact with pathogen-exposed workers, by the total number of contacts with pathogen-exposed workers, or by the cumulated duration of contacts pathogen-exposed workers (see Table S2).

Statistical analyses

All statistical tests used were two-sided and, when relevant, adjusted for multiple comparisons using the Benjamini-Hochberg method (53).

To compare the properties of the observed networks and their corresponding randomized null-model networks (pre-treatment period), we first averaged the focal property over all time windows (eight 3-hour windows covering the final 24 hours of the pre-treatment period) for each colony and for each of the observed and the 100 randomized contact sequences. We then performed a randomization test for each colony by comparing the observed value to the distribution of the 100 random values. This produced a one-sided p-value for each of the 22 analyzed colonies, ranging from 0 (when all random values were greater than the observed value) to 1 (when all

random values were lower than the observed value). These 22 one-sided p-values were then combined following a conservative meta-analysis method (Edgington's '*mean p*' method (54), implemented in R package 'metap'), producing a final two-sided p-value.

To evaluate the relationship between disease risk behavior (measured by proxy as the proportion of time spent inside) and network position, we performed a General Linear Mixed Model (GLMM) with degree or path length to queen as dependent variable, proportion of time spent inside as main effect, and ant identity, colony identity and time of day as random factors. To evaluate the effect of treatment on collective behavior and/or global network property, we performed a GLMM with treatment (sham-treated vs. pathogen-exposed), period (pre-treatment vs. post-treatment) and their contact as main effects, and colony identity and time of day as random factors. To evaluate the effect of treatment on individual behavior, we performed a similar GLMM with (when relevant) task group and its interactions with period and treatment as additional main effects, and ant identity as an additional random factor. To compare simulation results between pre-treatment and post-treatment networks, we used similar GLMMs, but without time of day as random factor. To compare the probability of worker contamination as a function of age, we performed a GLMM with binomial error structure using contamination as independent variable (i.e., fungal spores detected or not in the qPCR), worker age as main effect, and colony as random effect. Finally, to compare the measured fungal load of individuals as a function of caste sensu lato (queen vs. nurses vs. foragers), we first calculated the average load of each caste, then performed a GLMM with caste as a main effect, and colony as random effect. For all GLMM, we checked the normality of the model residuals using the following method: if there were fewer than 300 data points (collective behavior and global network properties), we performed a Shapiro-Wilks test. If there were more than 300 data points, the Shapiro-Wilks test and other normality tests were not

suitable to test normality of residuals, as they are too conservative (55). Instead, we used an alternative method (55), whereby the distribution of the residuals is considered to follow a normal distribution if its skewness is between -3 and +3 and its excess kurtosis is below 4. Whenever necessary, we performed standard data transformation (log, square-root, and power) to ensure that the residuals were normally distributed. When such transformation was performed, we plotted the transformed data rather than the original data in the figures.

We used a Kolmogorov-Smirnov test to compare the distribution of simulated pathogen loads between simulations performed over post-treatment and pre-treatment network.

To explore the association between disease transmission and network properties, we used a partial least square regression (R package ‘pls’) to model how the proportion of untreated workers that became contaminated (prevalence) and the mean pathogen load they received varied depending on the global properties of the observed post-treatment networks (modularity, clustering, efficiency, task assortativity, diameter, mean degree, and density) and on colony size (Fig. S9). This analysis was performed using the 22 colonies for which individual loads were measured by qPCR one day after pathogen-exposure (i.e., the 11 pathogen-exposed colonies from the main experiment and the 11 colonies from the age experiment). The aim of this analysis was not to establish a causal relationship between each network property and transmission, which would have required the experimental manipulation of network properties under carefully controlled conditions, but to get a joint overview of the effect direction and relative effect magnitude of the different variables. The partial least square regression approach is appropriate for datasets with relatively low sample size relative to the number of explanatory variables and high inter-correlation between the explanatory variables, as was the case in this analysis. The number of components used was determined as the one that minimized the bias-corrected cross-

validation estimate. Validation of the model was performed by testing the statistical significance of the association between fitted and measured values.

Survival analysis

Overall, the survival of untreated workers was high (>85% by the end of the experiment). However, visual inspection of the survival curve revealed an apparent increase in the mortality of untreated workers around 4 days after treatment. To test whether this increase was statistically significant, we fitted a piecewise exponential survival model following the method developed by Woolridge (2002) (56) and adapted for R by German Rodriguez (57). We found that the mortality rate of untreated workers during the first four days after treatment did not differ from their mortality rate before treatment (Hazard Ratio HR=1.05, p=0.89). By contrast, the mortality rate of untreated workers *after* these first four days post-treatment was significantly higher than their mortality rate before treatment (Hazard Ratio HR=2.95, p<0.0001). To more accurately quantify the additional mortality of untreated workers induced by pathogen exposure, we fitted a survival regression model to the pre-treatment period to extract the baseline mortality rate in our experimental conditions. We then used this fitted model to predict the survival of untreated workers at two time points: four days after treatment (i.e., before the pathogen-induced increase in untreated mortality), and at the end of the experiment. At four days after treatment, we found a very good fit between the predicted (94.9%) and observed survival (95.2%) of untreated workers, validating our approach. At the end of the experiment, the predicted ‘baseline’ survival among untreated workers was 90.7%, while the observed survival was 85.2%, suggesting that cross-contamination from the pathogen-exposed individuals induced an increase in mortality of 5.5% among untreated workers over the nine days following exposure of their treated nestmates.

To establish the link between short-term contamination and long-term survival, we used our simulation model to predict the spore load of each individual at the same time as in our main experiment (i.e., based on the observed contacts of the ants within the first 1 day period after colony treatment), and tested for an association with long-term survival by fitting a mixed effects Cox proportional hazard model with simulated load (high vs. low) as main effect and colony as random effect for each of the following two periods: 0-4 days after treatment, and 4-9 days after treatment. There was no difference in the survival of workers predicted to receive a high vs. low load from 0-4 days after treatment (mixed Cox model: $HR=0.57$, $\chi^2=0.71$, $df=1$, $p=0.40$). By contrast, workers predicted to have a high load had a significantly higher mortality rate than workers predicted to have a low load after these first four days post-treatment ($HR=2.43$, $\chi^2=6.43$, $df=1$, $p=0.011$).

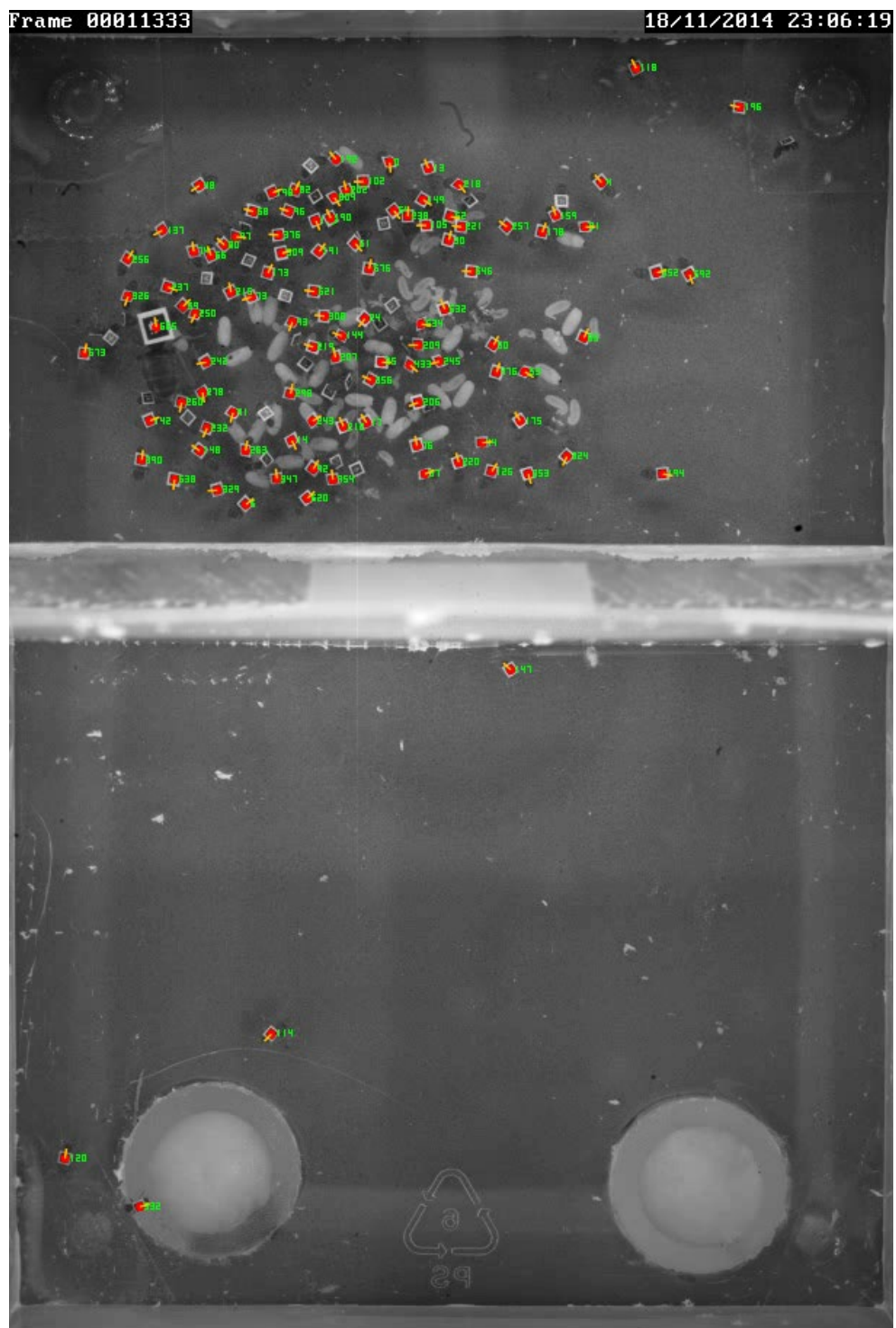


Fig. S1. Automated detection of a tagged *L. niger* colony in experimental conditions. The experimental arena was divided into a nest area (top) and a foraging area (bottom), separated by a central wall with a small entrance in the middle. The foraging area contained permanent sources of water and sugar water (bottom), which were provided via two cotton-stoppered plastic tubes connected to underneath containers, and whose opening was level with the foraging area's floor. Each detected ant is shown with a red dot, its unique identity displayed in green, and its orientation indicated by a yellow line.

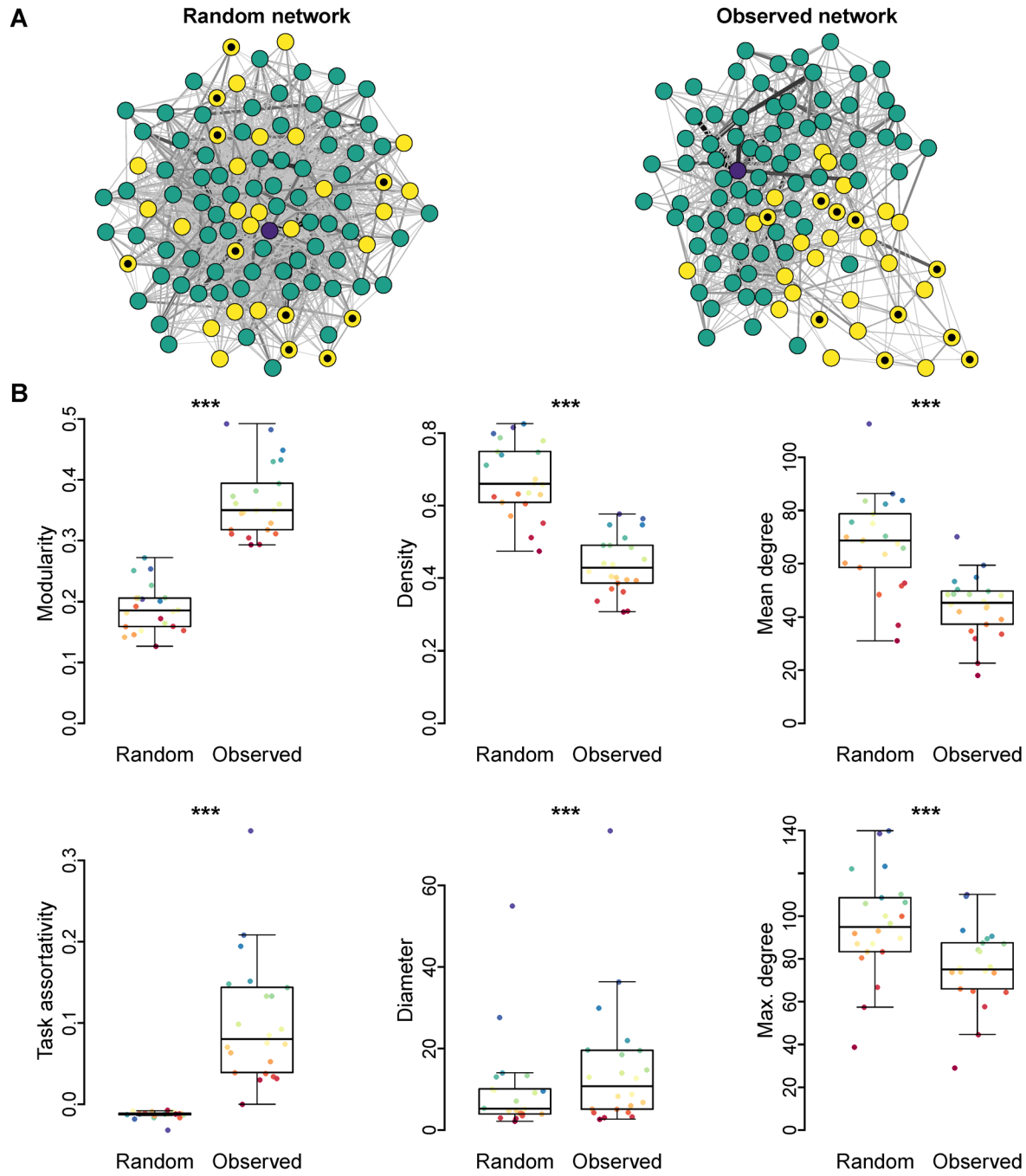


Fig. S2. Constitutive properties of the ant social networks compared to randomized networks. **A.** Example contact network from an experimental colony before treatment (right) and its corresponding randomized network (left). Each node represents an ant (queen: purple; indoor workers or nurses: green; outdoor workers or foragers: yellow). Weighted edges represent the cumulated duration of contact between each pair of ants. •: experimentally-treated foragers **B.** Comparison of the global properties of observed pre-treatment ant networks and their corresponding randomized networks. Thick lines represent the medians, boxes the interquartile ranges, whiskers the full range, and points the unique data points. Each colony is shown in a distinct color to facilitate comparisons. ***: $p < 0.0001$ in Edginton combined tests performed over individual randomization test results ($n=22$; see Table S1 for detail). The observed networks have significantly higher modularity, lower density, larger diameter, and lower mean and maximum degree than the corresponding random null model networks.

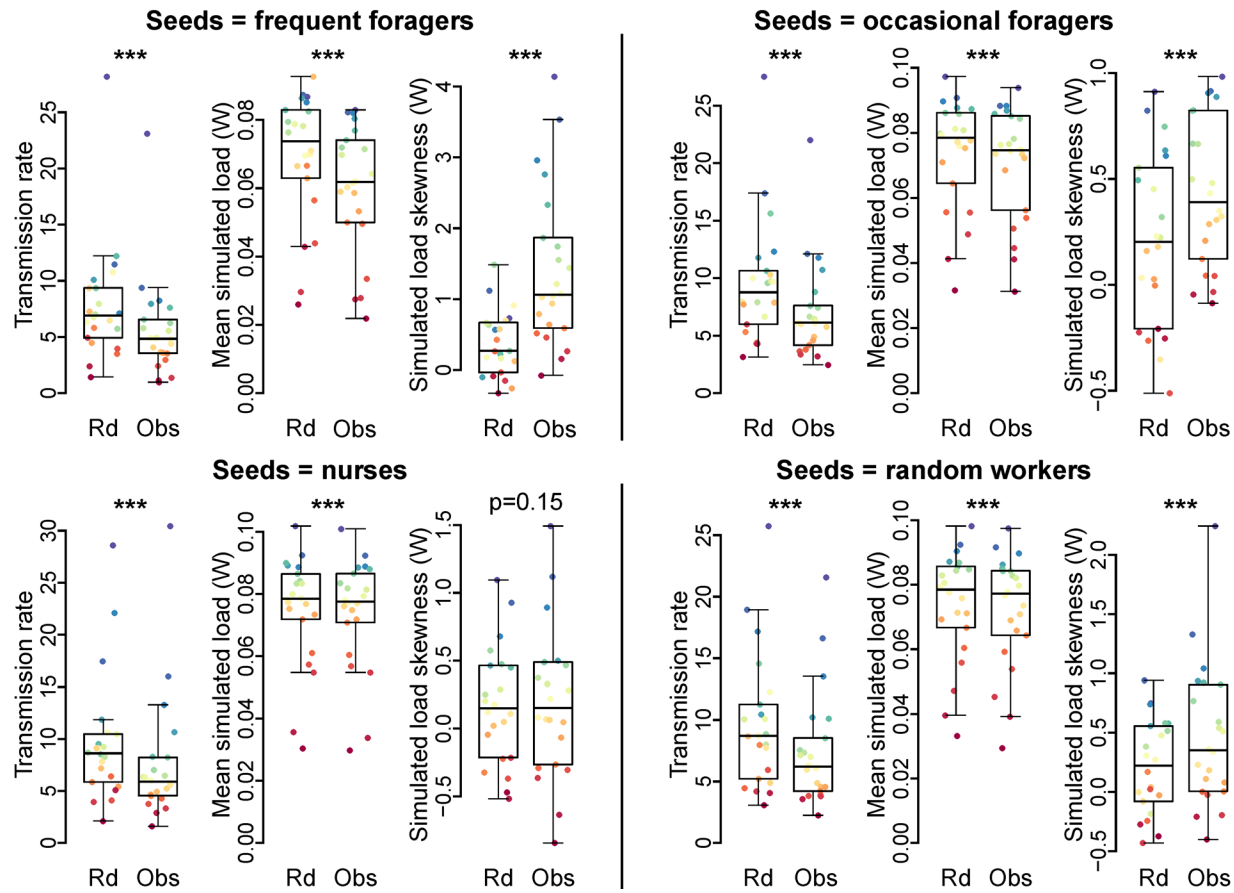


Fig. S3. Disease spread simulations over pre-treatment observed (Obs) and randomized (Rd) networks: colony-level results. Simulations started with a set of initially infectious ants (seeds), which were randomly selected among frequent foragers, occasional foragers, nurses, or all workers. The number of seeds in each colony was the same as the number of experimentally-treated ants. For each colony, we computed the transmission rate (r parameter in a r -K logistic equation fit over the first contamination times) and descriptive statistics (mean and skewness) for the distribution of simulated pathogen loads (total amount of pathogenic particles received during the simulation) among non-seed workers (W). Plotting conventions are the same as in Fig. S2. *: $p < 0.05$; **: $p < 0.01$; ***: $p < 0.0001$ in Edgington combined tests ($n=22$; see Table S1 for detail). Regardless of the identity of the seeds, simulated disease spread was significantly slower on observed than random networks (lower transmission rate) and resulted in significantly smaller amounts of pathogen transferred to nestmates (lower mean simulated pathogen loads). Additionally, the distribution of simulated pathogen loads among non-seed workers was always more right-skewed for the observed than the random networks, though this trend was not significant for nurse seeds. These results indicate that the properties of the ants' social networks consistently inhibit transmission.

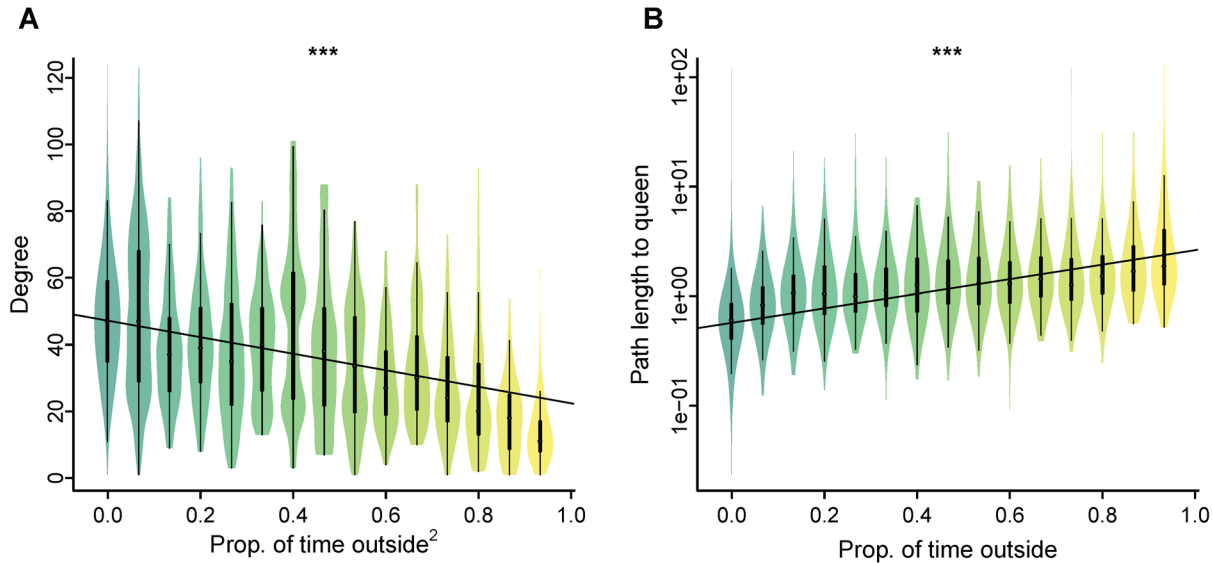


Fig. S4. Individual network position depending on time spent outside the nest. Relationship between the proportion of time each worker spends outside the nest and its degree (A) or its path length to the queen (B) in observed pre-treatment networks. White points represent the medians, thick black lines the interquartile ranges, thin black lines 1.5×the interquartile range, and violin shadings the density of individual data points. When relevant, the data transformation used to normalize residuals is indicated between brackets. General linear mixed models (GLMM), main effect of proportion of time spent outside, ***: $p < 0.0001$. There was a significant negative relationship between time spent outside (and thus, likelihood of encountering pathogens) and degree (number of connections within the network) and a significant positive relationship between time spent outside and path length (i.e., network distance) to the queen, indicating that workers that are at a higher risk of becoming infectious have lower spreading influence and are further away from the queen than workers that are at a lower risk of becoming infectious.

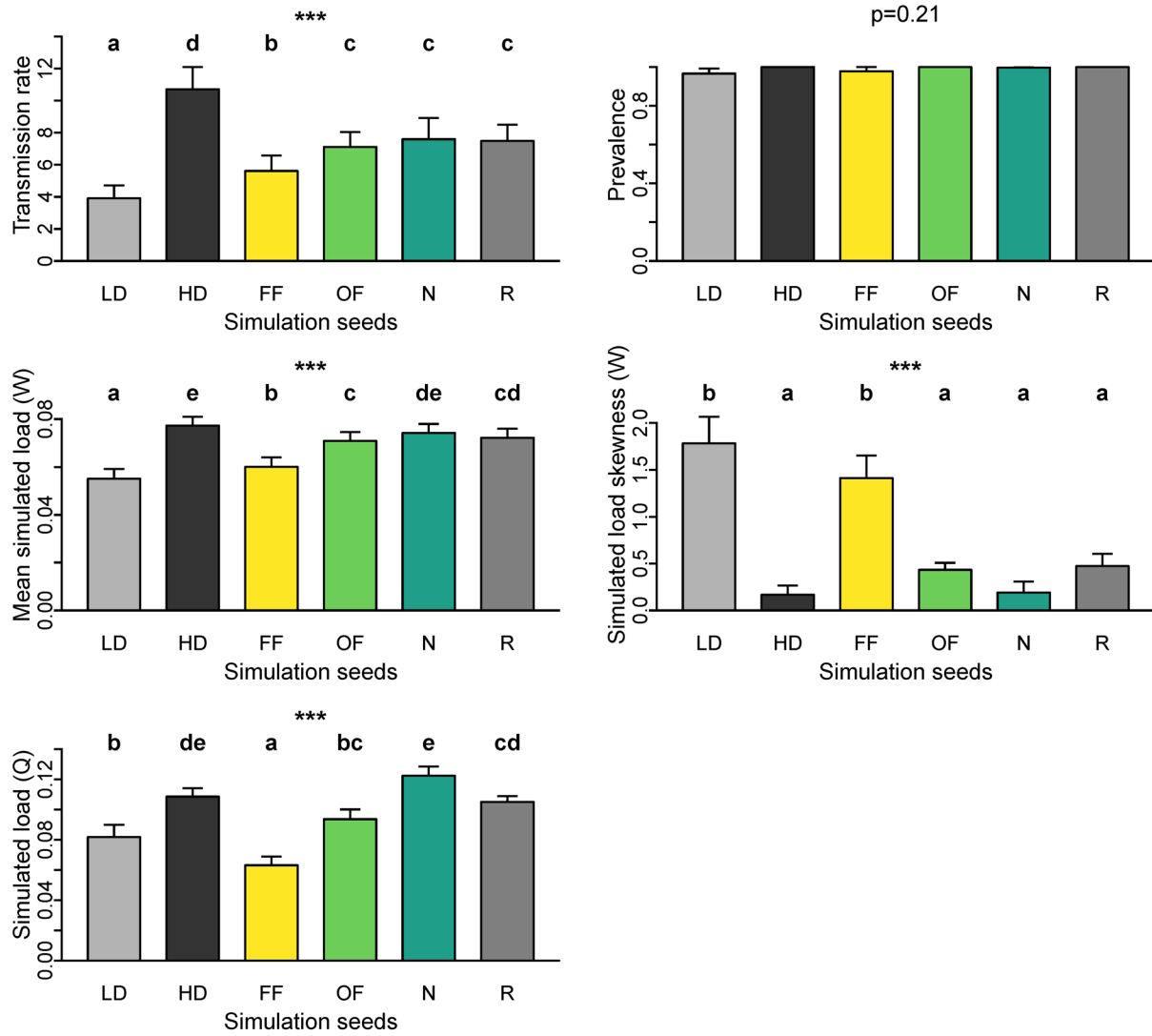


Fig. S5. Disease spread simulations run over pre-treatment observed networks: effect of disease origin. Simulations started with a set of initially infectious ants (seeds), which were randomly selected among low degree individuals (LD; light grey; 15% of workers with lowest degree within the network), high degree individuals (HD; black; 15% of workers with highest degree within the network), frequent foragers (FF; yellow; 50% of foragers that spent the larger proportion of their time outside; degree 41.9 ± 1.38), occasional foragers (OF; light green; 50% of foragers that spent the lower proportion of their time outside; degree 49.4 ± 1.04), nurses (N; dark green; workers that never left the nest; degree 46.9 ± 1.02), or all workers (R - random; dark grey, degree 45.4 ± 1.06). The number of seeds in each colony was the same as the number of experimentally-treated ants. For each colony, we computed the transmission rate (r parameter in a r-K logistic equation fit over the first contamination times), the prevalence (proportion of non-seed individuals that were contaminated during the simulation), descriptive statistics (mean and skewness) for the distribution of simulated pathogen loads (i.e., total amount of pathogenic particles received during the simulation) among non-seed workers (W), and the simulated pathogen load of the queen (Q). Bars and whiskers respectively represent the mean and standard errors of the variable of interest ($n=22$). ***: $p<0.0001$ in GLMM with seeds as a main effect and colony as a random effect. Same letters indicate no differences ($p>0.05$), and different letters significant differences ($p\leq 0.05$) in post-hoc comparisons with BH correction for multiple testing. Transmission was significantly more contained (i.e., slower transmission, transfer of smaller pathogen loads to both non-seed workers and the queen, and greater skew in load distribution among workers) when it originated from low-degree than from high-degree workers. Transmission was also significantly more contained when it originated from frequent foragers than when it originated from occasional foragers or nurses.

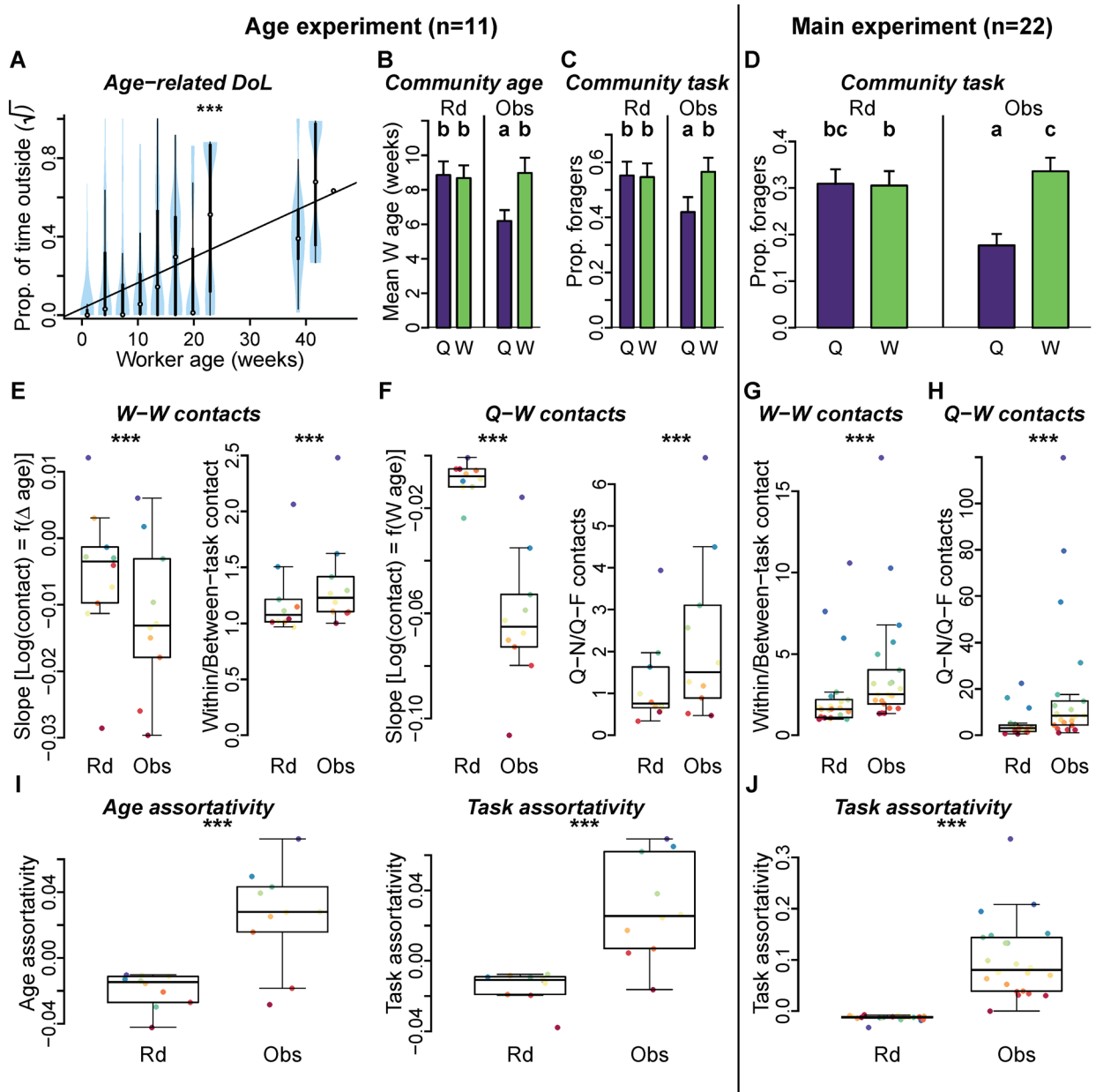


Fig. S6. Constitutive (i.e. pre-treatment) social organization of colonies in the age experiment (left; n=11 colonies) and the main experiment (right; n=22 colonies). Plotting conventions are as in Fig. S2 and S5. Note that the results on worker task are similar in both experiments, supporting their robustness. **A.** Proportion of time spent outside as a function of workers age. Mean age (**B**) and proportion of foragers (**C-D**) among workers that are part of the community containing the queen (Q, purple) or of a community containing workers only (W, green) in observed networks (Obs) and their corresponding randomized networks (Rd). **E, G.** Worker-worker (W-W) contacts. Slope of the relationship between total contact duration and age difference for each worker pair, and ratio of within-task (i.e., N-N and F-F) over between-task (i.e., N-F) contact duration (N: nurses, F: foragers). **F, H.** Queen-worker (Q-W) contacts. Slope of the relationship between worker age (W age) and total duration of contact with the queen, and ratio between the duration the queen spent in contact with nurses (Q-N) and the duration she spent in contact with foragers (Q-F). **I, J.** Age and task assortativity of the colony's social networks. *: p<0.05; **: p<0.01; ***: p<0.0001 in Edginton combined tests (random vs. observed comparisons; see Table S1 for detail), or GLMM with worker age as a main effect and colony as a random effect (violin plot). Same letters indicate no differences (p>0.05), and different letters significant differences (p<=0.05) in post-hoc comparisons with BH correction for multiple testing.

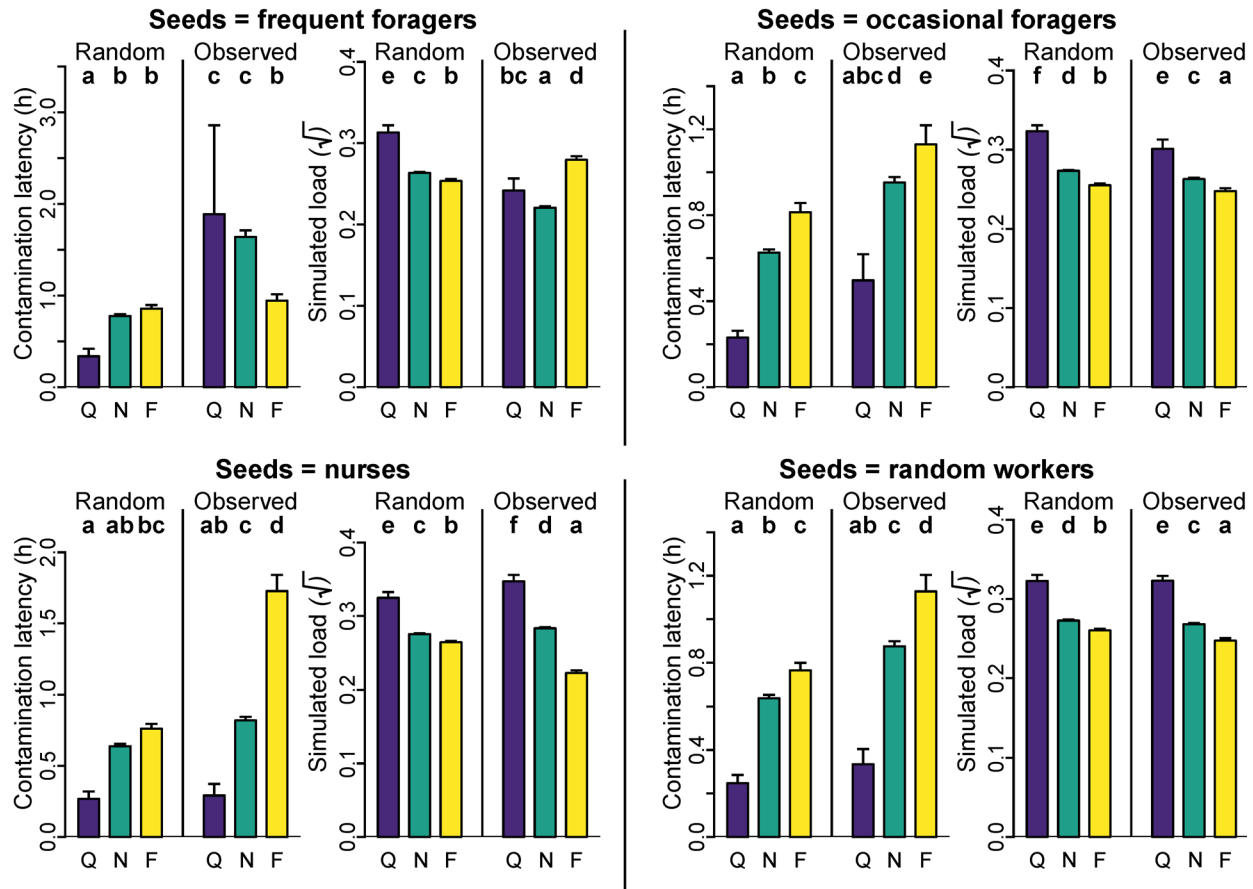


Fig. S7. Disease spread simulations run over pre-treatment observed (Obs) and randomized (Rd) networks: individual results. Simulations started with a set of initially infectious ants (seeds), which were randomly selected among frequent foragers, occasional foragers, nurses, or all workers. The number of seeds in each colony was the same as the number of experimentally-treated ants. Bars and whiskers respectively represent the means and standard errors of the plotted variables for each task group (Q: queen, N: non-seed nurses, F: non-seed foragers; untreated ants only). When relevant, the data transformation used to normalize residuals is indicated between brackets. Same letters indicate no differences ($p>0.05$), and different letters significant differences ($p\leq 0.05$) in post-hoc comparisons with BH correction for multiple testing. Simulations over observed networks were consistently associated with higher contamination latencies (i.e., first contamination times) and smaller amounts of pathogen transferred than random networks. However, the identity of the seeds significantly influenced the relative exposure risk of the queen, nurses and foragers. In all simulations over random networks, and in simulations over observed networks using random workers, nurses or occasional foragers as seeds, the queen and nurses had a significantly higher exposure risk than foragers, as shown by their lower contamination latency and their higher simulated pathogen load. This is presumably due to their high number of contacts. By contrast, in the most biologically plausible scenario (simulations over observed networks using frequent foragers as seeds), these trends were reversed, indicating that the queen and nurses had a significantly lower exposure risk than foragers. This indicates that the constitutive properties of the ants' social networks disproportionately protect high-value individuals (i.e., queen and young nurses) from the most likely source of disease (i.e., pathogens carried back to the colony by frequent foragers).

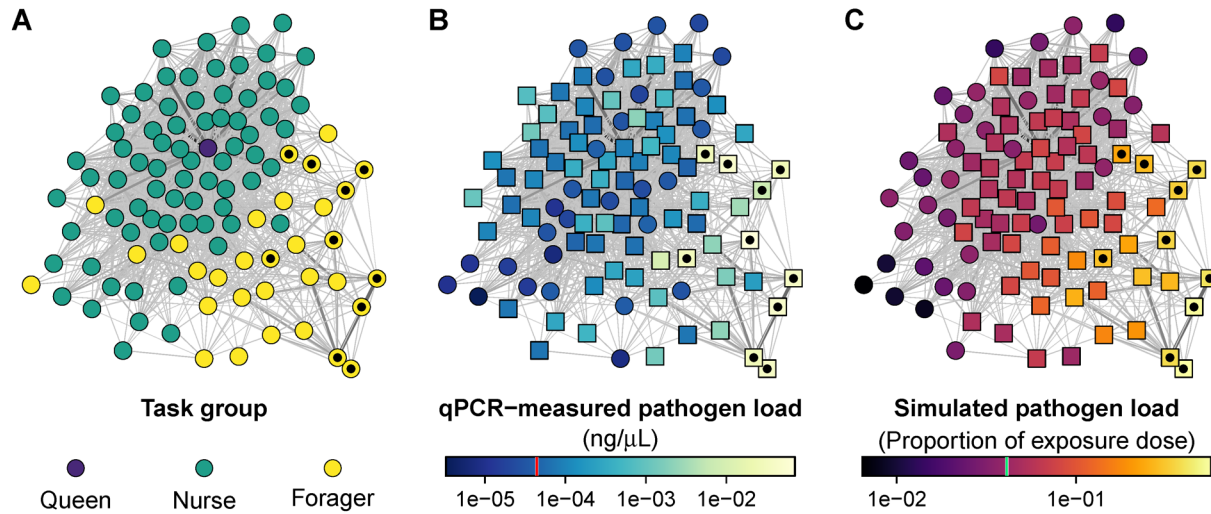


Fig. S8. Example post-treatment contact network in a pathogen-exposed colony. Each node represents an ant and weighted edges represent the cumulated duration of contact between each pair of ants. •: experimentally-treated foragers. Nodes are colored according to their task (A), their pathogen load as measured by qPCR one day following treatment (B), or their simulated pathogen load (C). Ants with high measured (B) or simulated (C) loads are represented by squares, whereas ants with low measured (B) or simulated (C) loads are represented by circles. The threshold values used to distinguish low loads from high load are the same as those in Fig. 2A and Fig. 3A, and are shown in red within the measured load color bar and in green within the simulated load color bar.

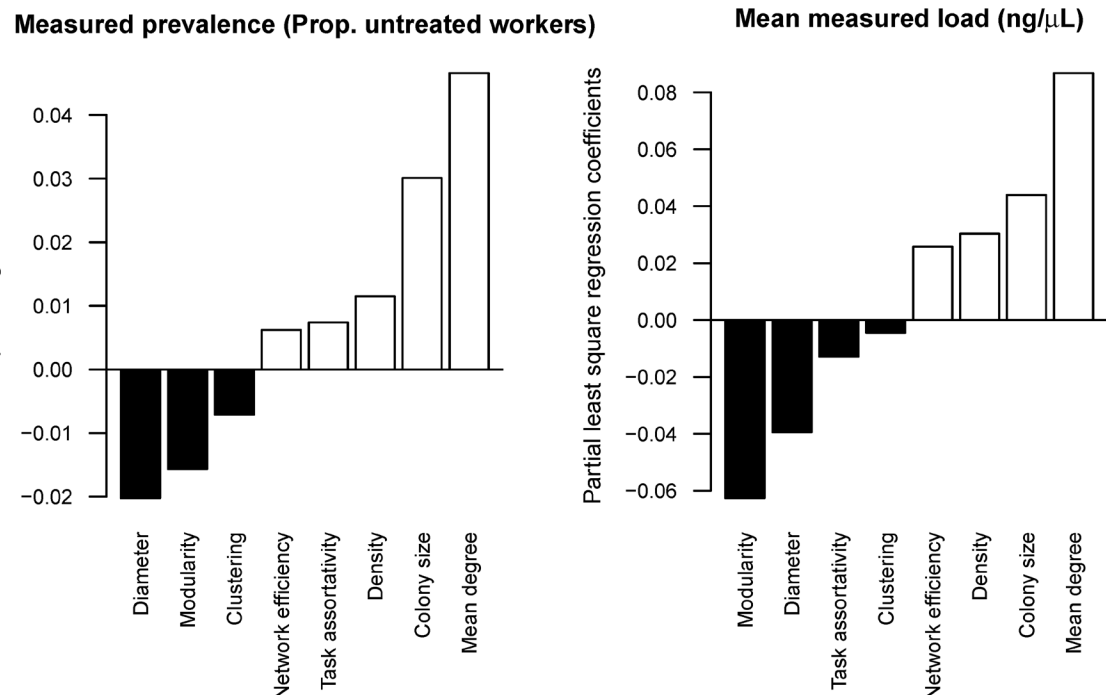
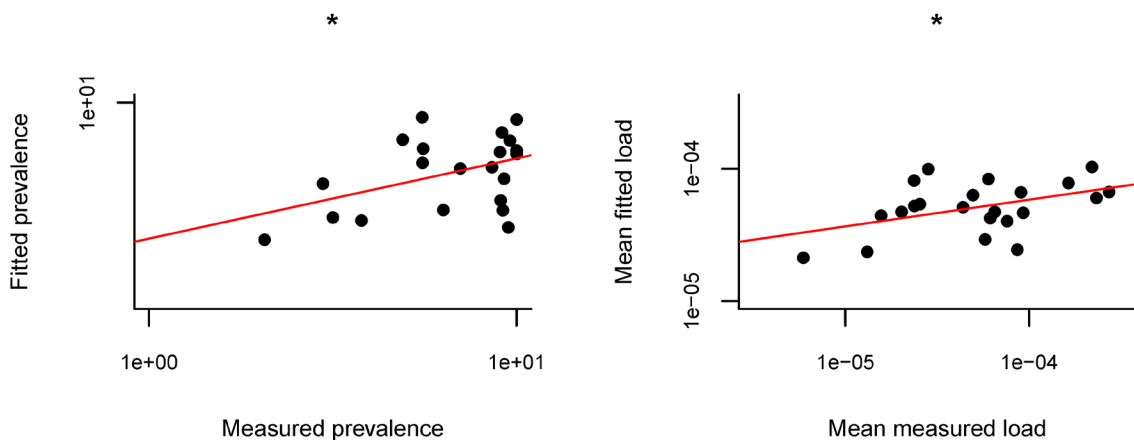
A**B**

Fig. S9. Measured prevalence and mean measured pathogen load among untreated workers as a function of post-treatment network properties in pathogen-exposed colonies ($n=11$ colonies from main experiment and 11 colonies from age experiment). **A.** Coefficients from partial least square regression models fitted using measured prevalence (left) or mean measured load (right) among untreated workers as dependent variable, and seven network properties plus colony size as explanatory variables. In both cases, a single component was retained, as it minimized the bias-corrected cross-validation estimate. Negative coefficients (black) indicate a transmission-inhibitory effect, while positive coefficients (white) indicate a transmission-enhancing effect. All effect directions are consistent with theoretical predictions: high modularity, diameter and clustering appear to inhibit disease transmission, while high network efficiency, density, colony size and mean degree appear to enhance disease transmission (see Table 1). Task assortativity (which has not been predicted to have a consistent effect on global disease transmission) was found to be associated with increased prevalence, but decreased mean received load. Note that this analysis is correlative and cannot establish a statistically significant causal relationship for each property. **B.** Relationship between measured and fitted values, calculated using the fitted partial least square regression models. Regression analysis reveals a significant positive association between measured and fitted values for both prevalence and mean measured loads, validating the predictive power of the models.

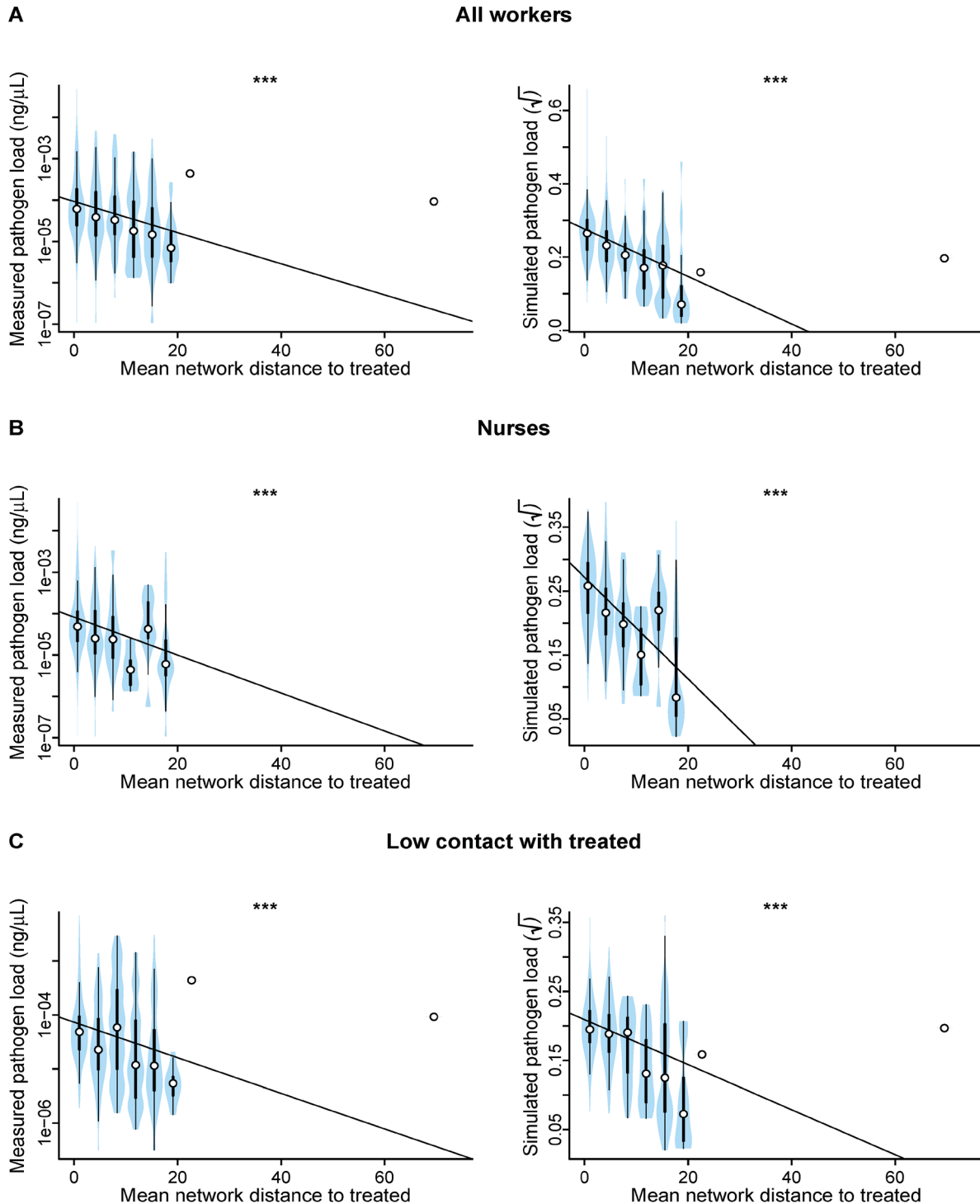


Fig. S10. Pathogen load as a function of network distance to treated foragers. Relationship between individual pathogen load measured by qPCR (left) or predicted by simulations (right) depending on the mean path length (i.e. network distance) to treated foragers measured from the post-treatment networks of pathogen-exposed colonies in the main experiment ($n=11$) and the age experiment ($n=11$). Data is shown for all untreated workers (A), for nurses only (B) and for workers with low direct contact with direct foragers only (C). B and C highlight the value of using a whole network approach to predict the contamination risk of individuals that have minimal direct contact with pathogen-exposed ants. General linear mixed models (GLMM) with colony as random factor, main effect of network distance to treated, ***: $p < 0.0001$, **: $p < 0.005$. Plotting conventions as in Fig. S4.

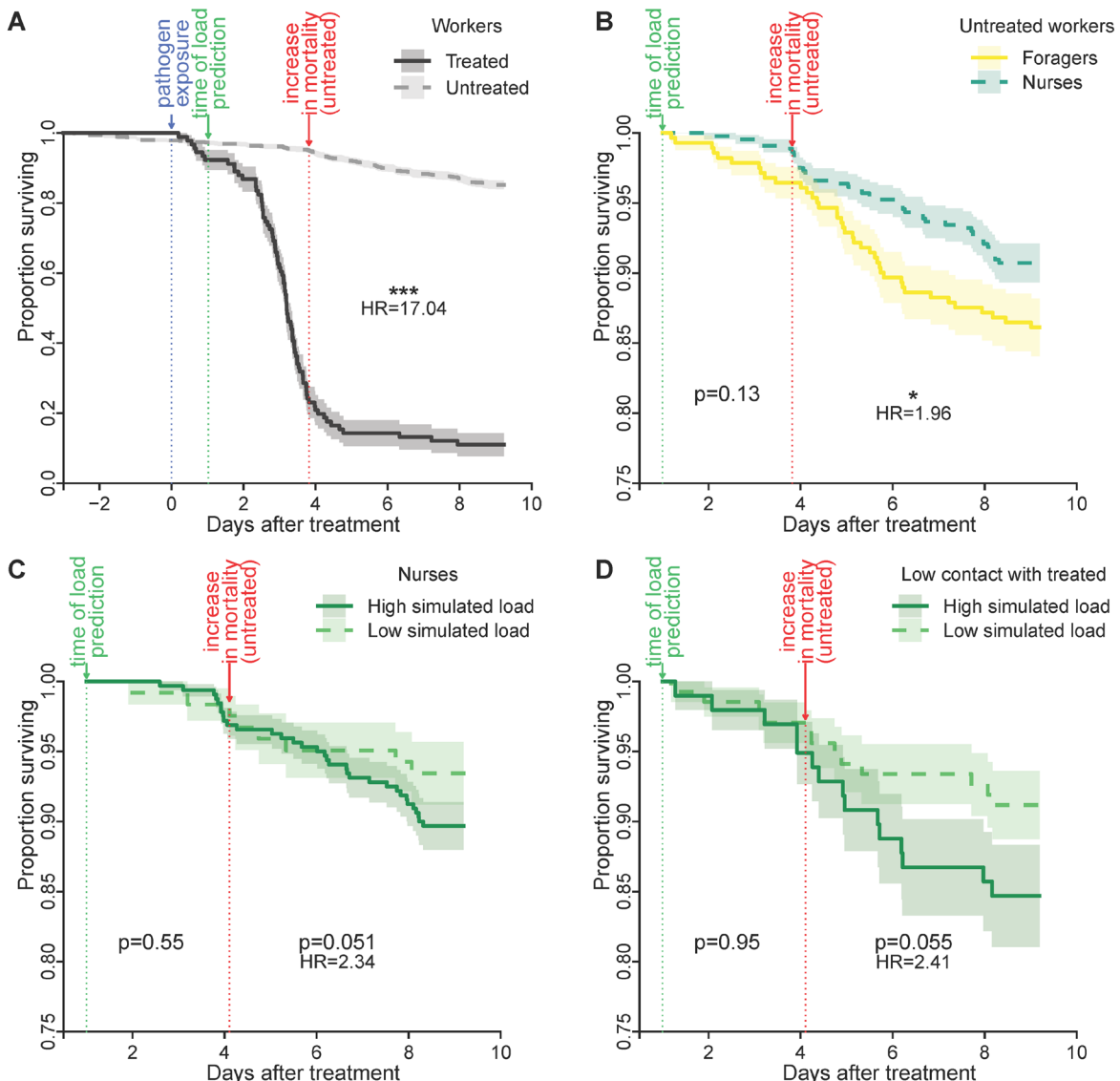


Fig. S11. Survival experiment ($n=11$ pathogen-exposed colonies including 11 queens, 778 untreated workers and 91 treated workers). Survival (lines) \pm 95% confidence intervals (shaded areas) of (A) treated (black, solid line) vs. untreated workers (grey, dashed line); (B) untreated foragers (yellow, solid line) vs. nurses (green, dashed line); (C) nurses predicted to receive a high (dark green, solid line) vs. low load (light green, dashed line) in simulations; (D) untreated workers with low direct contact with treated workers predicted to receive a high (dark green, solid line) vs. low load (light green, dashed line) in simulations. The dotted vertical lines show the time of treatment (blue, used as time origin), the time at which individual pathogen load was predicted based on simulations (green), and the time at which a significant increase in mortality was detected among untreated workers (red; c. 4 days after treatment). Fitting a piecewise exponential survival model revealed that the mortality rate of untreated workers (A) during the first four days after treatment did not differ from their mortality rate before treatment ($HR=1.05$, $z=0.14$, $p=0.89$). By contrast, the mortality rate of untreated workers *after* these first four days post-treatment was significantly higher than their mortality rate before treatment ($HR=2.95$, $z=4.05$, $p<0.0001$). The delay in pathogen-induced mortality among untreated workers relative to treated workers is likely due both to a delay in original contamination (time necessary for the spores to be transferred from treated to untreated workers), and to a possible slower development of the disease due to a lower initial contamination dose (cross-contamination rather than direct contamination). C and D underscore the value of our whole network simulation approach to predict the mortality risk of individuals that have minimal direct contact with treated workers. HR: Hazard ratio; ***: $p<0.0001$, *: $p<0.05$ in mixed effects Cox proportional hazard models with colony as random effect, fitted to the entire experiment (A) or fitted separately for the first four days after treatment and after day 4 (B-D). All queens were still alive at the end of the experiment.

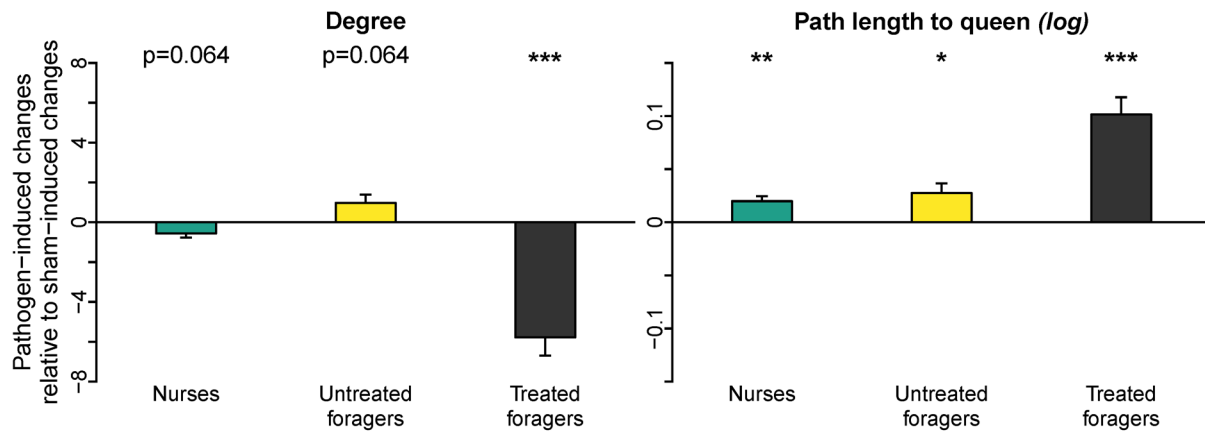


Fig. S12. Pathogen-induced changes in individual position within the network. Plotting conventions are the same as in the main text: for visual representation, bars and whiskers represent the means and standard errors of the difference between post- and pre-treatment values in pathogen-exposed colonies, from which the mean difference between post- and pre-treatment values in sham-exposed colonies was deducted. Statistical analyses were however performed on all raw data. GLMM, post-hoc comparisons of pathogen-induced and sham-induced changes, *: p<0.05; **: p<0.01; ***: p<0.0001 (after BH correction for multiple testing). When relevant, the data transformation used to normalize residuals is indicated between brackets.

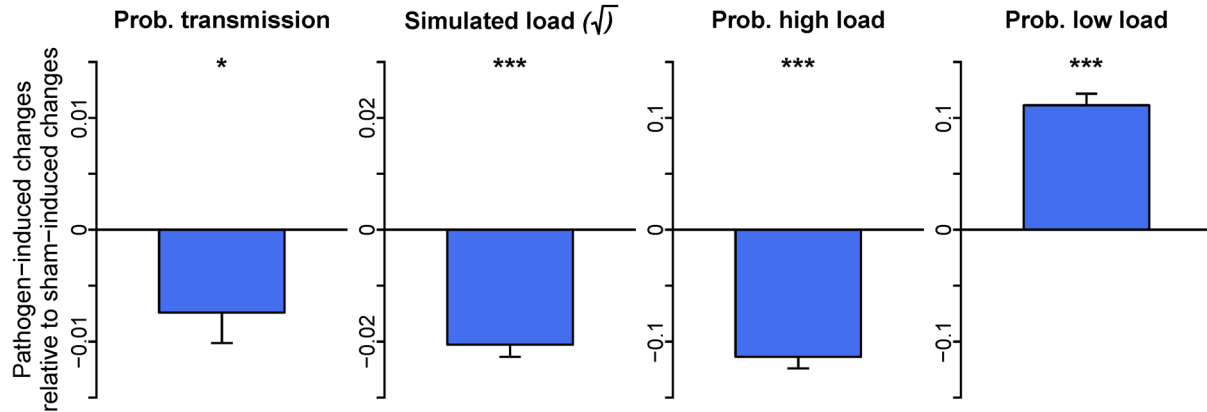


Fig. S13. Pathogen-induced changes in simulated disease transmission. Plotting conventions are the same as in the main text: for the visual representation, bars and whiskers represent the means and standard errors of the difference between post- and pre-treatment values in pathogen-exposed colonies, from which the mean difference between post- and pre-treatment values in sham-exposed colonies was deducted. Statistical analyses were however performed on all raw data. GLMM, interaction_{period (pre vs. post-treatment) × treatment (sham- vs. pathogen-exposed)}, *: $p < 0.05$; ***: $p < 0.0001$. When relevant, the data transformation used to normalize residuals is indicated between brackets.

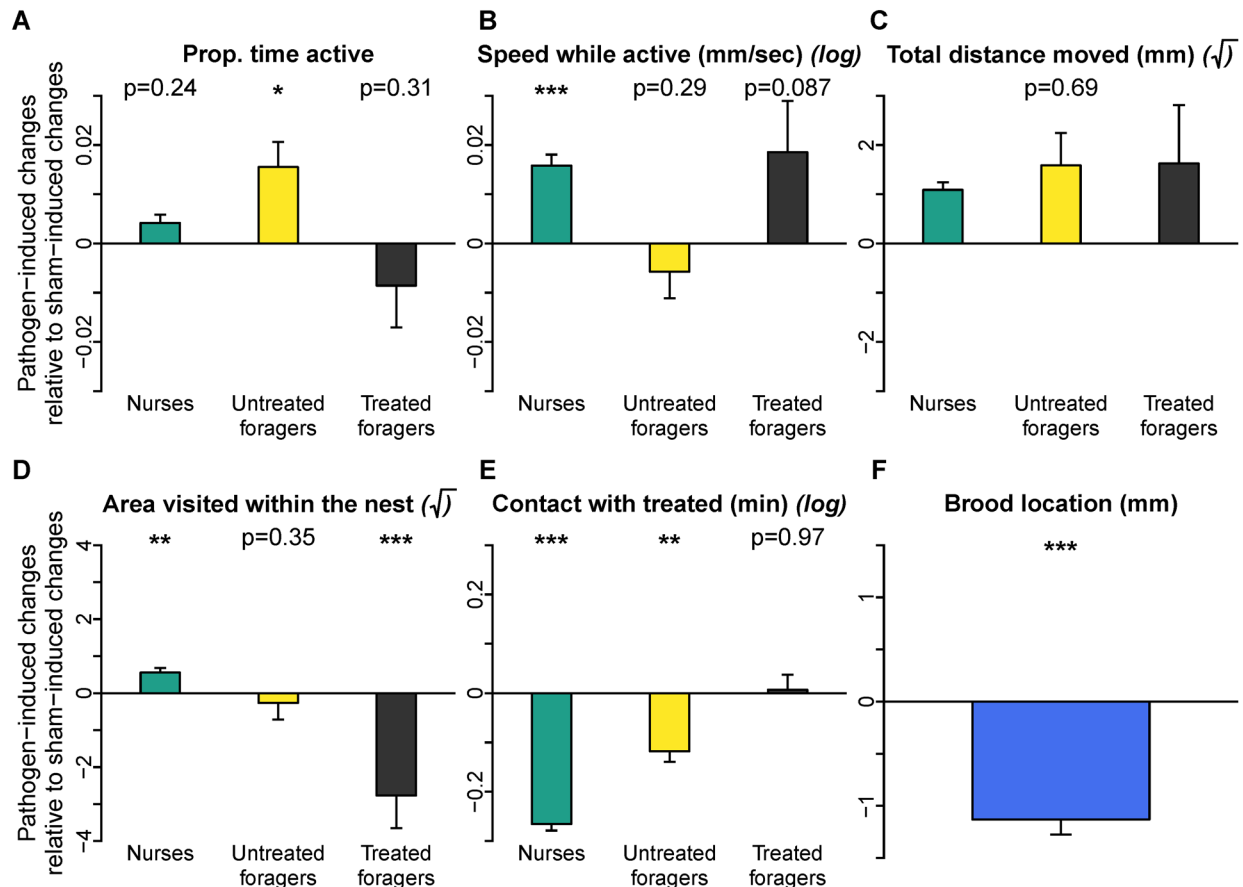


Fig. S14. Pathogen-induced changes in individual behavior. Plotting conventions are the same as in the main text: for visual representation, bars and whiskers represent the means and standard errors of the difference between post- and pre-treatment values in pathogen-exposed colonies, from which the mean difference between post- and pre-treatment values in sham-exposed colonies was deducted. The brood location (in mm) corresponds to the signed distance between the center of gravity of the brood pile and the nest entrance, with negative values corresponding to locations *inside* the nest and positive values to locations *outside* the nest. Statistical analyses were performed on all raw data. GLMM, interaction_{period (pre vs. post-treatment) × treatment (sham- vs. pathogen-exposed) × task (C); post-hoc comparisons of pathogen-induced and sham-induced changes, *: p<0.05; **: p<0.01; ***: p<0.0001 after BH correction for multiple testing (A-B, D-E); interaction_{period (pre vs. post-treatment) × treatment (sham- vs. pathogen-exposed), ***: p<0.0001 (F).} When relevant, the data transformation used to normalize residuals is indicated between brackets. Pathogen exposure did not induce changes in the overall activity levels of the treated foragers (A-C). By contrast, pathogen exposure induced a decrease in the area (in square mm) occupied by pathogen-exposed workers when inside the nest (D), a decrease in contact time between untreated individuals and treated workers (E), and a shift of the brood pile deeper within the nest (F).}

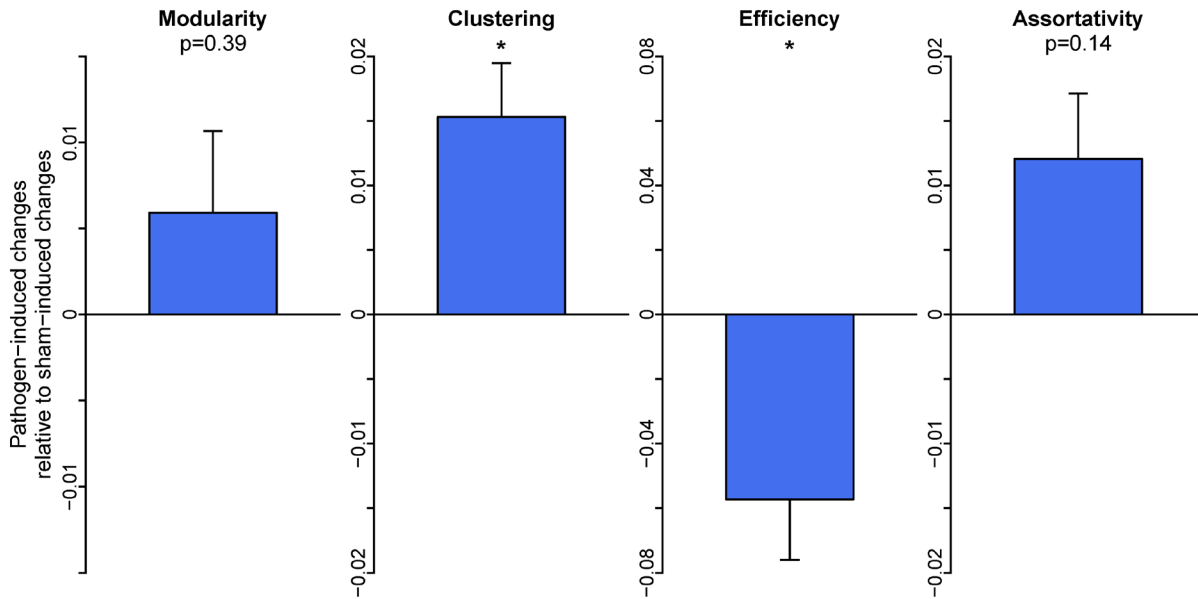


Fig. S15. Pathogen-induced changes in the social networks of untreated ants. Plotting conventions are the same as in the main text: for the visual representation, bars and whiskers represent the means and standard errors of the difference between post- and pre-treatment values in pathogen-exposed colonies, from which the mean difference between post- and pre-treatment values in sham-exposed colonies was deducted. Statistical analyses were however performed on all raw data. Modularity: $\chi^2=0.74$, df=1, $p\leq 0.39$; clustering: $\chi^2\geq 5.16$, df=1, $p\leq 0.023$; network efficiency: $\chi^2=4.35$, df=1, $p=0.037$; task assortativity: $\chi^2=2.13$, df=1, $p=0.14$. In this analysis, all experimentally-treated workers were removed from both pre-treatment and post-treatment networks so as to specifically evaluate the effect of pathogen-induced changes in the behavior of untreated ants on the network.

Fig. S2			
Colony	Modularity	Task ass.	Diameter
1	+ 0	+ 0	+ 0.02
2	+ 0	+ 0	+ 0.06
3	+ 0	+ 0	+ 0
4	+ 0	+ 0	+ 0.01
5	+ 0	+ 0	+ 0.23
6	+ 0	+ 0	+ 0.31
7	+ 0	+ 0	+ 0.26
8	+ 0	+ 0	+ 0
9	+ 0	+ 0	+ 0.01
10	+ 0	+ 0	+ 0.02
11	+ 0	+ 0	+ 0.26
12	+ 0	+ 0	+ 0.17
13	+ 0	+ 0	+ 0.34
14	+ 0	+ 0	+ 0.08
15	+ 0	+ 0	+ 0.09
16	+ 0	+ 0	+ 0.18
17	+ 0	+ 0	+ 0
18	+ 0	+ 0	+ 0
19	+ 0	+ 0	+ 0.02
20	+ 0	+ 0	+ 0.02
21	+ 0	+ 0	+ 0.05
22	+ 0	+ 0	+ 0.16
z	8.12	8.12	6.43
1-sided p	2.3·10 ⁻¹⁶	2.3·10 ⁻¹⁶	6.3·10 ⁻¹¹
2-sided p	4.5·10 ⁻¹⁶	4.5·10 ⁻¹⁶	1.3·10 ⁻¹⁰

Fig. S3			
Colony	Seeds = Frequent Foragers	Seeds = Occasional Foragers	
Colony	Transmission rate	Simulated W load	Transmission rate
1	- 0	- 0	- 0
2	- 0	- 0	- 0.03
3	- 0	- 0	- 0
4	- 0	- 0	- 0
5	- 0	- 0	- 0
6	- 0	- 0	- 0
7	+ 0.94	+ 0.02	- 0
8	- 0	- 0	- 0
9	- 0	- 0	- 0
10	- 0	- 0	- 0.01
11	+ 0.89	+ 0.05	- 0.13
12	- 0	- 0	- 0
13	- 0	- 0	- 0
14	- 0	- 0	- 0
15	- 0.02	- 0	- 0.17
16	- 0	- 0	- 0
17	- 0	- 0	- 0
18	- 0	- 0	- 0
19	- 0	- 0	- 0
20	- 0	- 0	- 0
21	- 0	- 0	- 0
22	- 0	- 0	- 0.26
z	6.76	8.12	8.07
1-sided p	7.0·10 ⁻¹²	2.3·10 ⁻¹⁶	3.4·10 ⁻¹⁶
2-sided p	1.4·10 ⁻¹¹	4.5·10 ⁻¹⁶	6.9·10 ⁻¹⁶

Seeds = Nurses				Seeds = Random workers		
Colony	Transmission rate	Simulated W load	Skew.	Transmission rate	Simulated W load	Skew.
1	- 0	- 0	- 0	- 0	- 0.22	+ 0
2	- 0.01	- 0.14	+ 0	- 0	- 0.01	+ 0
3	- 0	- 0.02	+ 0.2	- 0	- 0	+ 0
4	- 0	- 0.02	- 1	- 0.28	- 0	+ 0
5	- 0.04	- 0	+ 0.34	- 0.16	- 0	+ 0
6	- 0	- 0	- 1	- 0	- 0	+ 0
7	- 0	- 0.02	+ 0.14	- 0.02	- 0	+ 0
8	- 0.01	- 0.01	+ 0.33	- 0.01	- 0.09	- 0.93
9	- 0.02	- 0	- 0.8	- 0.01	- 0	+ 0.06
10	- 0	- 0	- 0.74	- 0	- 0	- 1
11	- 0	- 0	+ 0.01	- 0	- 0	+ 0
12	- 0	- 0.19	+ 0.36	- 0.48	- 0	+ 0
13	- 0.15	- 0	+ 0.01	- 0.03	- 0.13	+ 0.11
14	- 0	- 0.3	+ 0.07	- 0	- 0	- 0.72
15	- 0.17	- 0.26	- 0.99	- 0.1	- 0	+ 0
16	- 0	+ 0.93	- 0.93	- 0	- 0.06	+ 0
17	- 0	- 0	+ 0.04	- 0	- 0	+ 0
18	- 0	+ 0.51	+ 0.1	- 0	- 0	+ 0
19	- 0	- 0	+ 0.12	- 0	- 0.01	+ 0.02
20	+ 0.82	+ 0.95	- 0.99	- 0	- 0	+ 0.08
21	- 0	- 0.02	- 0.74	- 0	- 0	+ 0.01
22	- 0.12	- 0	+ 0.15	- 0	- 0	+ 0.18
z	7.13	5.64	1.43	7.32	7.74	5.83
1-sided p	4.9·10 ⁻¹³	8.7·10 ⁻⁹	0.07	1.2·10 ⁻¹³	5.0·10 ⁻¹⁵	2.8·10 ⁻⁹
2-sided p	9.7·10 ⁻¹³	1.7·10 ⁻⁸	0.15	2.5·10 ⁻¹³	9.9·10 ⁻¹⁵	5.6·10 ⁻⁹

Fig. S6				
Colony	Task ass.	Within / between contacts	Q-N/Q-F contacts	
1	+ 0	+ 0	+ 0	+ 0
2	+ 0	+ 0	+ 0	+ 0
3	+ 0	+ 0	+ 0	+ 0
4	+ 0	+ 0	+ 0	+ 0
5	+ 0	+ 0	+ 0	+ 0
6	+ 0	+ 0	+ 0	+ 0
7	+ 0	+ 0	+ 0	+ 0
8	+ 0	+ 0	+ 0	+ 0
9	+ 0	+ 0	+ 0	+ 0
10	+ 0	+ 0	+ 0	+ 0
11	+ 0	+ 0	+ 0	+ 0
12	+ 0	+ 0	+ 0	+ 0
13	+ 0	+ 0	+ 0	+ 0
14	+ 0	+ 0	+ 0	+ 0
15	+ 0	+ 0	+ 0	+ 0
16	+ 0	+ 0	+ 0	0.01
17	+ 0	+ 0	+ 0	+ 0
18	+ 0	+ 0	+ 0	+ 0
19	+ 0	+ 0	+ 0	+ 0
20	+ 0	+ 0	+ 0	+ 0
21	+ 0	+ 0	+ 0	+ 0
22	+ 0	+ 0	+ 0	+ 0
z	8.12	8.12	8.12	
1-sided p	2.3·10 ⁻¹⁶	2.3·10 ⁻¹⁶	2.4·10 ⁻¹⁶	
2-sided p	4.5·10 ⁻¹⁶	4.5·10 ⁻¹⁶	4.8·10 ⁻¹⁶	

Fig. S6						
Colony	Task ass.	Within / between contacts	Q-N/Q-F contacts	W-W contacts = f(Δage)	Q-W contacts = f(W age)	Age ass.
A1	+ 0	+ 0.04	+ 0	1	0	+ 0.01
A2	+ 0	- 0.87	0.98	- 0.18	0	+ 0
A4	+ 0	+ 0.01	+ 0	- 0.02	- 0	+ 0.04
A5	+ 0	+ 0	+ 0	- 0	- 0	+ 0
A6	+ 0	+ 0	+ 0	- 0	- 0	+ 0
A7	+ 0	+ 0	+ 0	- 0	- 0	+ 0
A8	+ 0	- 0.91	+ 0	- 0.4	- 0	+ 0
A9	+ 0	+ 0	+ 0	- 0	- 0	+ 0
A10	+ 0	+ 0	+ 0	- 0	- 0	+ 0
A11	+ 0	+ 0	+ 0	- 0	- 0	+ 0
z	5.48	3.4	4.31	3.72	5.48	5.42
1-sided p	2.2·10 ⁻⁸	0.00026	8.3·10 ⁻⁶	9.8·10 ⁻⁵	2.2·10 ⁻⁸	2.9·10 ⁻⁸
2-sided p	4.3·10 ⁻⁸	0.00052	1.7·10 ⁻⁵	0.00020	4.3·10 ⁻⁸	5.9·10 ⁻⁸

Table S1. Randomization test results. Effect direction (+ or -: observed value respectively greater or lower than the median of the 100 random values) and significance (proportion of random values that are respectively lower or greater than the observed values) for each colony and each variable shown in Fig. S2, S3 and S6. For each variable, the test statistic (z), one-sided and two-sided combined p-values computed using Edgington's 'mean p' method are provided. Colonies 1-22 correspond to the main experiment and Colonies A1-A11 to the age experiment. Ass.: network assortativity, Skew.: skewness, W: worker, Q: queen, N: nurse, F: forager.

Explanatory variable	MEASURED LOAD												SURVIVAL	
	All workers						Untreated workers only						Untreated workers only	
	Per colony			Pooled			Per colony			Pooled			Per colony	Pooled
	ρ	AIC	R ²	ρ	AIC	R ²	ρ	AIC	R ²	ρ	AIC	R ²	AIC	AIC
Simulation model Simulated load	0.67±0.02	224.5±16	0.45±0.02	0.61	5326	0.48	0.291±0.03	172.8±15	0.110±0.02	0.40	4132	0.355	55.6±25	789
Alternative Model 1 Contact/no contact with treated workers					6387	0.13					4324	0.279		
Alternative Model 2 No. contacts with treated workers	0.21±0.05	265±18	0.15±0.03	0.34	6044	0.27	0.170±0.04	173.5±15	0.107±0.02	0.30	4177	0.339	57.0±24	799
Alternative Model 3 Duration of contacts with treated workers	0.21±0.06	271.3±18	0.11±0.03	0.32	6186	0.21	0.170±0.05	176.1±15	0.082±0.02	0.34	4231	0.318	57.2±24	801

Table S2. Comparison of the predictive value of the simulation model with simpler predictive models. The table presents the Pearson correlation coefficient (ρ), AIC (Akaike information criterion) and the R² (coefficient of determination) for multiple predictive models, allowing a comparison of their goodness-of-fit (ρ , higher lower AIC and higher R² values indicate a better model fit). Models were fitted either for each of the 22 colonies separately ('Colony-by-colony') or for all 22 colonies pooled ('All colonies pooled'). In all models, contacts were defined using the '*front contacts*' with truncation method (see Methods and Table S4). The left part of the table presents predictive models of the 'measured load', i.e., the amount of *Metarhizium brunneum* on each worker, measured by qPCR 26 hours after contamination of 10% of the colony's workforce (see Methods; pathogen-exposed colonies in the main experiment: n=11; age experiment: n=11). For the colony-by-colony analyses, we fitted a general linear model using the log-transformed measured load of each workers as dependent variable. The explanatory variable used was (i) the log-transformed simulated load (outcome of our simulation model), (ii) a categorical variable encoding whether or not each ant had been in contact with pathogen-exposed workers (Alternative Model 1), (iii) the square-root transformed total number of contacts with pathogen-exposed workers (Alternative Model 2), or (iv) the log-transformed cumulated duration of contacts with pathogen-exposed workers. For the pooled analyses, we fitted a general linear mixed-model using the same specifications, with colony identity as a random factor. The transformation retained for each explanatory variable was the one that provided the best fit with the data while ensuring normality of the model residuals. Only 2 out of 22 colonies included individuals that had no contacts with pathogen-exposed workers, so the colony-specific results are not given for this model. The right part of the table presents predictive models of untreated worker survival in the survival experiment (see Methods; n=11 colonies). For all analyses, we fitted a Cox proportional hazard model with untreated worker survival as dependent variable and, for the pooled analyses, colony identity as a random factor. We used the same explanatory variables as for the 'measured load' models, and retained the variable transformations that provided the best fit with the data (simulation model: no transformation; number of contacts: log-transformation; duration of contact: square-root transformation). Note that in that experiment, all workers came into contact with treated foragers at least once, so we could not fit Alternative Model 1.

	Variable	Main effect	χ^2	df	p	post-hoc effect	z	p (BH)
Pre-exposure organization	Degree	Prop. of time outside (sqrt)	402.88	1	$2.2 \cdot 10^{-16}$	-	-	-
	Path length to Q (log)	Prop. of time outside	908.41	1	$2.2 \cdot 10^{-16}$	-	-	-
	Prop. of time outside (sqrt)	Age	144.39	1	$2.2 \cdot 10^{-16}$	-	-	-
	Mean worker age	Community×Network	36.45	1	$1.6 \cdot 10^{-9}$	Q - other, random Q - other , observed	0.51 -8.02	0.72 $6.7 \cdot 10^{-15}$
	Prop. foragers (age exp.)	Community	34.29	1	$4.8 \cdot 10^{-9}$	Q - other , random Q - other , observed	0.31 -7.97	0.76 $9.3 \cdot 10^{-15}$
	Prop. foragers (main exp.)	Community	73.29	1	$2.2 \cdot 10^{-16}$	Q - other , random Q - other , observed	0.27 -11.8	0.78 $<1 \cdot 10^{-08}$
Contamination	Measured load (log)	Task	28.05	2	$8.1 \cdot 10^{-7}$	N - Q F - Q F - N	0.05 4.61 4.56	0.96 $7.6 \cdot 10^{-06}$ $7.6 \cdot 10^{-06}$
Fit simulations-data	Simulated load (log)	Measured load (log)	361.1	1	$2.2 \cdot 10^{-16}$	-	-	-
Network changes, collective	Modularity	Period×Treatment	10.36	1	0.0013	-	-	-
	Clustering coefficient	Period×Treatment	5.85	1	0.016	-	-	-
	Network efficiency	Period×Treatment	5.27	1	0.022	-	-	-
	Task assortativity	Period×Treatment	4.25	1	0.039	-	-	-
Network changes, individual	Degree	Period×Treatment×Task	46.43	2	$8.3 \cdot 10^{-11}$	ΔN path. - ΔN sham ΔF path. - ΔF sham ΔT path. - ΔT sham	-1.85 1.87 -6.84	0.064 0.064 $2.3 \cdot 10^{-11}$
	Path length to Q (log)	Period×Treatment×Task	14.67	2	0.00065	ΔN path. - ΔN sham ΔF path. - ΔF sham ΔT path. - ΔT sham	2.9 2.16 5.11	0.0056 0.031 $9.9 \cdot 10^{-07}$
Behavioral changes, collective	Brood pile location	Period×Treatment	22.68	1	$1.9 \cdot 10^{-6}$	-	-	-
Behavioral changes, individual	Prop. of time outside (power)	Period×Treatment×Task	60.25	2	$8.2 \cdot 10^{-14}$	ΔN path. - ΔN sham ΔF path. - ΔF sham ΔT path. - ΔT sham	1.63 3.54 8.77	0.1 0.00061 $<1 \cdot 10^{-08}$
	Distance to colony (log)	Period×Treatment×Task	98.22	2	$2.2 \cdot 10^{-16}$	ΔN path. - ΔN sham ΔF path. - ΔF sham ΔT path. - ΔT sham	1.27 3.74 10.94	0.2 0.00027 $<1 \cdot 10^{-08}$
	Overlap with brood	Period×Treatment×Task	16.91	2	0.00021	ΔN path. - ΔN sham ΔF path. - ΔF sham ΔT path. - ΔT sham	4.43 0.06 -2.47	$2.6 \cdot 10^{-05}$ 0.95 0.02
	Inter-task contact (sqrt)	Period×Treatment	17.35	1	$3.1 \cdot 10^{-5}$	-	-	-
	Prop. time active	Period×Treatment×Task	6.49	2	0.039	ΔN path. - ΔN sham ΔF path. - ΔF sham ΔT path. - ΔT sham	1.4 2.92 -1.01	0.24 0.01 0.31
	Speed while active (log)	Period×Treatment×Task	10.09	2	0.0064	ΔN path. - ΔN sham ΔF path. - ΔF sham ΔT path. - ΔT sham	4.36 -1.05 1.9	$4 \cdot 10^{-05}$ 0.29 0.087
	Distance moved (sqrt)	Period×Treatment×Task	2	2	0.79	-	-	-
	Area visited within the nest (sqrt)	Period×Treatment×Task	45.52	2	$1.3 \cdot 10^{-10}$	ΔN path. - ΔN sham ΔF path. - ΔF sham ΔT path. - ΔT sham	3.34 -0.93 -5.82	0.0013 0.35 $1.8 \cdot 10^{-08}$
	Contact with T (log)	Period×Treatment×Task	34.01	2	$4.1 \cdot 10^{-8}$	ΔN path. - ΔN sham ΔF path. - ΔF sham ΔT path. - ΔT sham	-14.4 -3.61 0.04	$<1 \cdot 10^{-08}$ 0.00047 0.97
Simulation changes, collective	Prob. contamination (power)	Period×Treatment	6.30	1	0.012	-	-	-
	Final infectivity (sqrt)	Period×Treatment	43.27	1	$4.8 \cdot 10^{-11}$	-	-	-
	Prob. high load	Period×Treatment	59.72	1	$1.1 \cdot 10^{-14}$	-	-	-
	Prob. low load	Period×Treatment	56.82	1	$4.8 \cdot 10^{-14}$	-	-	-
Simulation changes, individual	Prob. high load, Q (power)	Period×Treatment	5.78	1	0.016	-	-	-
	Prob. high load, W (power)	Period×Treatment×Task	22.66	2	$1.2 \cdot 10^{-5}$	ΔN path. - ΔN sham ΔF path. - ΔF sham	-8.38 -0.58	$<1 \cdot 10^{-08}$ 0.56
	Prob. low load, Q (sqrt)	Period×Treatment	5.08	1	0.024	-	-	-
	Prob. low load, W (sqrt)	Period×Treatment×Task	23.77	2	$6.9 \cdot 10^{-6}$	ΔN path. - ΔN sham ΔF path. - ΔF sham	9.02 0.37	$<1 \cdot 10^{-08}$ 0.71

Table S3. GLMM statistics. When relevant, the data transformation used to normalize the model residuals is indicated between brackets (log: logarithm, sqrt: square-root). For the inter-task contact, the two-way interaction Period×Treatment is reported because the three-way interaction Period×Treatment×Task was not significant. Q: queen, W: workers, N: nurses, F: untreated foragers, T: treated foragers, BH: Benjamini-Hochberg corrected.

Dipping suspension concentration (spores. mL ⁻¹)	Number of spores on body (mean ± s.e.)	Pathogen-induced mortality after 12 days in isolation
10 ⁵	33 ± 11	1.5%
10 ⁶	120 ± 16	7.6%
10 ⁷	1588 ± 342	17.7%
10 ⁸	20650 ± 2801	34.4%
10 ⁹	238667 ± 29978	49.2%

Table S4. Dose-response data for the *Lasius neglectus*–*Metarhizium brunneum* host-pathogen system (communicated by Matthias Konrad and Sina Metzler). 1032 *L. neglectus* workers were individually dipped into one of six solutions: a sham solution of 0.05% Triton-X, and five *M. brunneum* (strain MA275, KVL 03-143, as in the rest of the study) spore suspensions in 0.05% Triton-X at the respective concentrations of 10⁵, 10⁶, 10⁷, 10⁸, and 10⁹ spores.mL⁻¹. Workers were then placed on filter paper for a few seconds until recovery, then they were either freeze-killed at -20°C for spore count determination (60 workers per concentration), or transferred to sterile Petri dishes in which they were reared alone for 12 days for mortality determination (72 ants per concentration). For the spore count determination, pools of 10 ants (6 pools per concentration) were washed by vortexing in 1mL 0.05% Triton X, followed by additional rinsing. The elution suspension was then centrifuged for 5 min at full speed, then the supernatant was pipetted out and the remaining spore pellets were re-suspended in 20µL (10⁵ and 10⁶ spore.mL⁻¹ suspensions) or 50µL (10⁷, 10⁸ and 10⁹ spore suspensions) 0.05% Triton-X. The spore concentrations of the resulting suspensions were then determined using a cell counter (Cellometer ® Auto M10), and used to calculate the number of spores on the body of each ant. For the mortality determination, all ants were provided with 10% sucrose throughout the experiment, and kept at 23°C and 75% humidity with a 14h:10h light/dark cycle. Survival was checked daily for 12 days. To establish whether mortality was caused induced by the pathogen, dead ants were surface-sterilized in ethanol and sodium hypochlorite, then placed on moist filter paper in a Petri dish at constant temperature (23°C). Cadavers were checked daily for a period of 3 weeks for outgrowth of *M. brunneum* (19). All ants that died from natural causes (i.e., ants for which no fungal outgrowth was detected after death) were excluded from the calculation of pathogen-induced mortality. The Table shows the mean ± standard error of the number of spores per ant for each dipping suspension concentration, and the corresponding pathogen-induced mortality. In these experimental conditions, a mean of 33 spores per ant (which is close to our estimated threshold value of 35 spores per ants; see ‘Quantification of pathogen load’ section) was found to lead to an excess mortality of 1.52% (i.e., lethal dose of c. 2% or LD2). Note that this mortality value is valid for *L. neglectus* workers reared in isolation, but may differ for *L. niger* workers reared within the colony, where they can receive sanitary care from nestmates.

Contact inference method	Truncate d contacts	All workers							Untreated workers only						
		Best model	Per colony			Pooled			Best model	Per colony			Pooled		
			AIC	R ²	ρ	AIC	R ²	ρ		AIC	R ²	ρ	AIC	R ²	ρ
front contacts	yes	13	224.5±16	0.451±0.02	0.667±0.02	5326	0.481	0.612	8	172.8±15	0.110±0.02	0.291±0.03	4132	0.355	0.400
front contacts	no	1	226.0±16	0.443±0.02	0.660±0.02	5350	0.475	0.608	4	173.1±15	0.108±0.02	0.285±0.04	4137	0.353	0.395
front and back contacts	yes	0	228.8±17	0.432±0.02	0.651±0.02	5413	0.458	0.596	3	173.5±15	0.104±0.02	0.282±0.03	4141	0.351	0.394
front and back contacts	no	1	230. 1±17	0.425±0.03	0.645±0.02	5428	0.454	0.593	2	173.7±15	0.103±0.02	0.278±0.03	4143	0.350	0.392
any overlap	yes	5	229.8±17	0.431±0.03	0.649±0.02	5422	0.456	0.594	4	173.7±15	0.105±0.02	0.285±0.03	4139	0.352	0.391
any overlap	no	2	231.7±17	0.419±0.03	0.640±0.02	5450	0.448	0.588	1	174.2±15	0.099±0.02	0.273±0.03	4149	0.348	0.384

Table S5. Comparison of the predictive value of the simulation model using different contact inference methods. The table presents the fit between experimentally measured and predicted pathogen loads for pathogen-exposed colonies in the main experiment ($n=11$) and in the age experiment ($n=11$). Simulations were run for each combination of contact inference method ('front contacts' vs. 'front and back contacts' vs. 'any overlap') and truncation ('yes': contacts between immobile ants truncated after 2 minutes; 'no': no truncation). For each series of simulations, we fitted a general linear model to the measured pathogen load as a function of the simulated pathogen load for each of the 22 colonies individually ('Colony-by-colony'), and a general linear mixed-model with colony identity as a random factor for all 22 colonies pooled together ('All colonies pooled'). We then extracted each model's AIC and R², and calculated the Pearson correlation coefficient (ρ) between measured and simulated loads (note that both measured and simulated loads were log-transformed to ensure normality of the model's residuals). Lower AIC and higher R² values indicate a better model fit. For each series of simulations, we provide (i) the number of colonies in which the combination considered gave the best fit between simulated and experimental data (i.e. lowest AIC) out of all 6 tested combinations; (ii) the mean ± standard error of the AIC, R², and Pearson correlation coefficients for the 22 colony-specific fitted models; and (iii) the AIC, R² and Pearson correlation coefficient for the models fitted on the entire dataset (pooled across all 22 colonies). The combination presenting the best fit with the experimental data, which was retained for all analyses, is highlighted in green.

References and Notes

1. M. Barthélemy, A. Barrat, R. Pastor-Satorras, A. Vespignani, Dynamical patterns of epidemic outbreaks in complex heterogeneous networks. *J. Theor. Biol.* **235**, 275–288 (2005).
[doi:10.1016/j.jtbi.2005.01.011](https://doi.org/10.1016/j.jtbi.2005.01.011) [Medline](#)
2. K. T. D. Eames, M. J. Keeling, Modeling dynamic and network heterogeneities in the spread of sexually transmitted diseases. *Proc. Natl. Acad. Sci. U.S.A.* **99**, 13330–13335 (2002).
[doi:10.1073/pnas.202244299](https://doi.org/10.1073/pnas.202244299) [Medline](#)
3. R. K. Hamede, J. Bashford, H. McCallum, M. Jones, Contact networks in a wild Tasmanian devil (*Sarcophilus harrisii*) population: Using social network analysis to reveal seasonal variability in social behaviour and its implications for transmission of devil facial tumour disease. *Ecol. Lett.* **12**, 1147–1157 (2009). [doi:10.1111/j.1461-0248.2009.01370.x](https://doi.org/10.1111/j.1461-0248.2009.01370.x) [Medline](#)
4. J. O. Lloyd-Smith, S. J. Schreiber, P. E. Kopp, W. M. Getz, Superspreading and the effect of individual variation on disease emergence. *Nature* **438**, 355–359 (2005).
[doi:10.1038/nature04153](https://doi.org/10.1038/nature04153) [Medline](#)
5. D. P. Mersch, A. Crespi, L. Keller, Tracking individuals shows spatial fidelity is a key regulator of ant social organization. *Science* **340**, 1090–1093 (2013).
[doi:10.1126/science.1234316](https://doi.org/10.1126/science.1234316) [Medline](#)
6. T. O. Richardson, T. E. Gorochowski, Beyond contact-based transmission networks: The role of spatial coincidence. *J. R. Soc. Interface* **12**, 20150705 (2015).
[doi:10.1098/rsif.2015.0705](https://doi.org/10.1098/rsif.2015.0705) [Medline](#)
7. T. O. Richardson, J. I. Liechti, N. Stroeymeyt, S. Bonhoeffer, L. Keller, Short-term activity cycles impede information transmission in ant colonies. *PLOS Comput. Biol.* **13**, e1005527 (2017). [doi:10.1371/journal.pcbi.1005527](https://doi.org/10.1371/journal.pcbi.1005527) [Medline](#)
8. P. Sah, S. T. Leu, P. C. Cross, P. J. Hudson, S. Bansal, Unraveling the disease consequences and mechanisms of modular structure in animal social networks. *Proc. Natl. Acad. Sci. U.S.A.* **114**, 4165–4170 (2017). [doi:10.1073/pnas.1613616114](https://doi.org/10.1073/pnas.1613616114) [Medline](#)
9. M. Salathé, J. H. Jones, Dynamics and control of diseases in networks with community structure. *PLOS Comput. Biol.* **6**, e1000736 (2010). [doi:10.1371/journal.pcbi.1000736](https://doi.org/10.1371/journal.pcbi.1000736) [Medline](#)
10. E. M. Volz, J. C. Miller, A. Galvani, L. A. Meyers, Correction: Effects of heterogeneous and clustered contact patterns on infectious disease dynamics. *PLOS Comput. Biol.* **7**, 10.1371/annotation/85b99614-44b4-4052-9195-a77d52dbdc05 (2011).
[doi:10.1371/annotation/85b99614-44b4-4052-9195-a77d52dbdc05](https://doi.org/10.1371/annotation/85b99614-44b4-4052-9195-a77d52dbdc05)
11. C. L. Nunn, F. Jordán, C. M. McCabe, J. L. Verdolin, J. H. Fewell, Infectious disease and group size: More than just a numbers game. *Philos. Trans. R. Soc. London B Biol. Sci.* **370**, 20140111 (2015). [doi:10.1098/rstb.2014.0111](https://doi.org/10.1098/rstb.2014.0111) [Medline](#)
12. S. Cremer, C. D. Pull, M. A. Fürst, Social Immunity: Emergence and evolution of colony-level disease protection. *Annu. Rev. Entomol.* **63**, 105–123 (2018). [doi:10.1146/annurev-ento-020117-043110](https://doi.org/10.1146/annurev-ento-020117-043110) [Medline](#)

13. S. Cremer, S. A. O. Armitage, P. Schmid-Hempel, Social immunity. *Curr. Biol.* **17**, R693–R702 (2007). [doi:10.1016/j.cub.2007.06.008](https://doi.org/10.1016/j.cub.2007.06.008) Medline
14. N. Stroeymeyt, B. Casillas-Pérez, S. Cremer, Organisational immunity in social insects. *Curr. Opin. Insect Sci.* **5**, 1–15 (2014). [doi:10.1016/j.cois.2014.09.001](https://doi.org/10.1016/j.cois.2014.09.001)
15. D. Naug, S. Camazine, The role of colony organization on pathogen transmission in social insects. *J. Theor. Biol.* **215**, 427–439 (2002). [doi:10.1006/jtbi.2001.2524](https://doi.org/10.1006/jtbi.2001.2524) Medline
16. D. Naug, B. Smith, Experimentally induced change in infectious period affects transmission dynamics in a social group. *Proc. Biol. Sci.* **274**, 61–65 (2007). [doi:10.1098/rspb.2006.3695](https://doi.org/10.1098/rspb.2006.3695) Medline
17. C. D. Pull, W. O. H. Hughes, M. J. F. Brown, Tolerating an infection: An indirect benefit of co-founding queen associations in the ant *Lasius niger*. *Naturwissenschaften* **100**, 1125–1136 (2013). [doi:10.1007/s00114-013-1115-5](https://doi.org/10.1007/s00114-013-1115-5) Medline
18. S. Angelone, M. J. Bidochka, Diversity and abundance of entomopathogenic fungi at ant colonies. *J. Invertebr. Pathol.* **156**, 73–76 (2018). [doi:10.1016/j.jip.2018.07.009](https://doi.org/10.1016/j.jip.2018.07.009) Medline
19. M. Konrad, M. L. Vyleta, F. J. Theis, M. Stock, S. Tragust, M. Klatt, V. Drescher, C. Marr, L. V. Ugelvig, S. Cremer, Social transfer of pathogenic fungus promotes active immunisation in ant colonies. *PLOS Biol.* **10**, e1001300 (2012). [doi:10.1371/journal.pbio.1001300](https://doi.org/10.1371/journal.pbio.1001300) Medline
20. T. Brütsch, G. Jaffuel, A. Vallat, T. C. J. Turlings, M. Chapuisat, Wood ants produce a potent antimicrobial agent by applying formic acid on tree-collected resin. *Ecol. Evol.* **7**, 2249–2254 (2017). [doi:10.1002/ece3.2834](https://doi.org/10.1002/ece3.2834) Medline
21. P. C. Lopes, P. Block, B. König, Infection-induced behavioural changes reduce connectivity and the potential for disease spread in wild mice contact networks. *Sci. Rep.* **6**, 31790 (2016). [doi:10.1038/srep31790](https://doi.org/10.1038/srep31790) Medline
22. S. Vestergaard, T. M. Butt, J. Bresciani, A. T. Gillespie, J. Eilenberg, Light and electron microscopy studies of the infection of the western flower thrips *Frankliniella occidentalis* (Thysanoptera: Thripidae) by the entomopathogenic fungus *Metarrhizium anisopliae*. *J. Invertebr. Pathol.* **73**, 25–33 (1999). [doi:10.1006/jipa.1998.4802](https://doi.org/10.1006/jipa.1998.4802) Medline
23. R. B. Rosengaus, J. F. A. Tranillo, T. Chen, J. J. Brown, R. D. Karp, Immunity in a social insect. *Naturwissenschaften* **86**, 588–591 (1999). [doi:10.1007/s001140050679](https://doi.org/10.1007/s001140050679)
24. L. Liu, G. H. Li, P. D. Sun, C. L. Lei, Q. Y. Huang, Experimental verification and molecular basis of active immunization against fungal pathogens in termites. *Sci. Rep.* **5**, 15106 (2015). [doi:10.1038/srep15106](https://doi.org/10.1038/srep15106) Medline
25. W. O. H. Hughes, J. Eilenberg, J. J. Boomsma, Trade-offs in group living: Transmission and disease resistance in leaf-cutting ants. *Proc. Biol. Sci.* **269**, 1811–1819 (2002). [doi:10.1098/rspb.2002.2113](https://doi.org/10.1098/rspb.2002.2113) Medline
26. N. Stroeymeyt, A. V. Grasse, A. Crespi, D. Mersch, S. Cremer, L. Keller, Social network plasticity decreases disease transmission in a eusocial insect. Zenodo (2018); <https://doi.org/10.5281/zenodo.1322669>.

27. N. Stroeymeyt, A. V. Grasse, A. Crespi, D. Mersch, S. Cremer, L. Keller, Social network plasticity decreases disease transmission in a eusocial insect. Zenodo (2018); <https://doi.org/10.5281/zenodo.1322676>.
28. V. Latora, M. Marchiori, Efficient behavior of small-world networks. *Phys. Rev. Lett.* **87**, 198701 (2001). [doi:10.1103/PhysRevLett.87.198701](https://doi.org/10.1103/PhysRevLett.87.198701) Medline
29. A. Bhatkar, W. H. Whitcomb, Artificial diet for rearing various species of ants. *Fla. Entomol.* **53**, 229 (1970). [doi:10.2307/3493193](https://doi.org/10.2307/3493193)
30. A. Sendova-Franks, N. R. Franks, Task allocation in ant colonies within variable environments (A study of temporal polyethism: Experimental). *Bull. Math. Biol.* **55**, 75–96 (1993). [doi:10.1007/BF02460295](https://doi.org/10.1007/BF02460295)
31. A. Reber, M. Chapuisat, Diversity, prevalence and virulence of fungal entomopathogens in colonies of the ant *Formica selysi*. *Insectes Soc.* **59**, 231–239 (2012). [doi:10.1007/s00040-011-0209-3](https://doi.org/10.1007/s00040-011-0209-3)
32. S. Keller, P. Kessler, C. Schweizer, Distribution of insect pathogenic soil fungi in Switzerland with special reference to *Beauveria brongniartii* and *Metharhizium anisopliae*. *BioControl* **48**, 307–319 (2003). [doi:10.1023/A:1023646207455](https://doi.org/10.1023/A:1023646207455)
33. J. Giehr, A. V. Grasse, S. Cremer, J. Heinze, A. Schrempf, Ant queens increase their reproductive efforts after pathogen infection. *R. Soc. Open Sci.* **4**, 170547 (2017). [doi:10.1098/rsos.170547](https://doi.org/10.1098/rsos.170547) Medline
34. M. Fiala, in *2005 IEEE International Workshop on Haptic, Audio and Visual Environments and Their Applications* (IEEE Computer Society Press, 2005), pp. 148–153.
35. B. Hölldobler, E. O. Wilson, *The Ants* (Harvard Univ. Press, 1990).
36. J. F. A. Traniello, Comparative foraging ecology of north temperate ants: The role of worker size and cooperative foraging in prey selection. *Insectes Soc.* **34**, 118–130 (1987). [doi:10.1007/BF02223830](https://doi.org/10.1007/BF02223830)
37. M. B. Thomas, A. F. Read, Can fungal biopesticides control malaria? *Nat. Rev. Microbiol.* **5**, 377–383 (2007). [doi:10.1038/nrmicro1638](https://doi.org/10.1038/nrmicro1638) Medline
38. S. Xavier-Santos, B. Magalhães, E. A. L.-A. Lima, Differentiation of the entomopathogenic fungus *Metarhizium flavoviride* (Hyphomycetes). *Rev. Microbiol.* **30**, 47–51 (1999). [doi:10.1590/S0001-37141999000100009](https://doi.org/10.1590/S0001-37141999000100009)
39. S. Aron, J. M. Pasteels, J. L. Deneubourg, J. L. Boeve, Foraging recruitment in *Leptothorax unifasciatus*: The influence of foraging area familiarity and the age of the nest-site. *Insectes Soc.* **33**, 338–351 (1986). [doi:10.1007/BF02224249](https://doi.org/10.1007/BF02224249)
40. R. James, D. Croft, J. Krause, Potential banana skins in animal social network analysis. *Behav. Ecol. Sociobiol.* **63**, 989–997 (2009). [doi:10.1007/s00265-009-0742-5](https://doi.org/10.1007/s00265-009-0742-5)
41. J. Heinze, B. Walter, Moribund ants leave their nests to die in social isolation. *Curr. Biol.* **20**, 249–252 (2010). [doi:10.1016/j.cub.2009.12.031](https://doi.org/10.1016/j.cub.2009.12.031) Medline
42. F. Barraquand, S. Benhamou, Animal movements in heterogeneous landscapes: Identifying profitable places and homogeneous movement bouts. *Ecology* **89**, 3336–3348 (2008). [doi:10.1890/08-0162.1](https://doi.org/10.1890/08-0162.1) Medline

43. J. Fieberg, C. O. Kochanny, Quantifying home-range overlap: The importance of the utilization distribution. *J. Wildl. Manage.* **69**, 1346–1359 (2005). [doi:10.2193/0022-541X\(2005\)69\[1346:QHOTIO\]2.0.CO;2](https://doi.org/10.2193/0022-541X(2005)69[1346:QHOTIO]2.0.CO;2)
44. V. D. Blondel, J.-L. Guillaume, R. Lambiotte, E. Lefebvre, Fast unfolding of communities in large networks. *J. Stat. Mech.* **2008**, P10008 (2008). [doi:10.1088/1742-5468/2008/10/P10008](https://doi.org/10.1088/1742-5468/2008/10/P10008)
45. A. Barrat, M. Barthelemy, A. Vespignani, in *Large Scale Structure and Dynamics of Complex Networks: From Information Technology to Finance and Natural Science*, vol. 2 of *Complex Systems and Interdisciplinary Science*, G. Caldarelli, A. Vespignani, Eds. (World Scientific, 2007), pp. 67–92.
46. M. E. Newman, Assortative mixing in networks. *Phys. Rev. Lett.* **89**, 208701 (2002). [doi:10.1103/PhysRevLett.89.208701](https://doi.org/10.1103/PhysRevLett.89.208701) Medline
47. M. E. Newman, Mixing patterns in networks. *Phys. Rev. E Stat. Nonlin. Soft Matter Phys.* **67**, 026126 (2003). [doi:10.1103/PhysRevE.67.026126](https://doi.org/10.1103/PhysRevE.67.026126) Medline
48. P. Holme, J. Saramäki, Temporal networks. *Phys. Rep.* **519**, 97–125 (2012). [doi:10.1016/j.physrep.2012.03.001](https://doi.org/10.1016/j.physrep.2012.03.001)
49. D. R. Farine, When to choose dynamic vs. static social network analysis. *J. Anim. Ecol.* **87**, 128–138 (2018). [doi:10.1111/1365-2656.12764](https://doi.org/10.1111/1365-2656.12764) Medline
50. L. E. C. Rocha, F. Liljeros, P. Holme, Information dynamics shape the sexual networks of Internet-mediated prostitution. *Proc. Natl. Acad. Sci. U.S.A.* **107**, 5706–5711 (2010). [doi:10.1073/pnas.0914080107](https://doi.org/10.1073/pnas.0914080107) Medline
51. L. E. C. Rocha, F. Liljeros, P. Holme, Simulated epidemics in an empirical spatiotemporal network of 50,185 sexual contacts. *PLOS Comput. Biol.* **7**, e1001109 (2011). [doi:10.1371/journal.pcbi.1001109](https://doi.org/10.1371/journal.pcbi.1001109) Medline
52. E. R. Pianka, On r- and K-selection. *Am. Nat.* **104**, 592–597 (1970). [doi:10.1086/282697](https://doi.org/10.1086/282697)
53. Y. Benjamini, Y. Hochberg, Controlling the false discovery rate: A practical and powerful approach to multiple testing. *J. R. Stat. Soc. B* **57**, 289–300 (1995).
54. R. Rosenthal, Combining results of independent studies. *Psychol. Bull.* **85**, 185–193 (1978). [doi:10.1037/0033-2909.85.1.185](https://doi.org/10.1037/0033-2909.85.1.185)
55. H.-Y. Kim, Statistical notes for clinical researchers: Assessing normal distribution (2) using skewness and kurtosis. *Restor. Dent. Endod.* **38**, 52–54 (2013). [doi:10.5395/rde.2013.38.1.52](https://doi.org/10.5395/rde.2013.38.1.52) Medline
56. J. M. Wooldridge, *Econometric Analysis of Cross Section and Panel Data* (MIT Press, 2002).
57. G. Rodríguez, Piecewise exponential models in R: Recidivism in the U.S. (2017); <http://data.princeton.edu/wws509/stata/recidivismR.html>.